Journal of Computational Physics 307 (2016) 423–445

Contents lists available at ScienceDirect

Journal of Computational Physics

www.elsevier.com/locate/jcp

Directly solving the Hamilton–Jacobi equations by Hermite WENO Schemes ☆

Feng Zheng, Jianxian Qiu *

School of Mathematical Sciences and Fujian Provincial Key Laboratory of Mathematical Modeling & High-Performance Scientific Computing, Xiamen University, Xiamen, Fujian 361005, PR China

ARTICLE INFO

Article history:
Received 7 September 2015
Received in revised form 24 November 2015
Accepted 1 December 2015
Available online 11 December 2015

Keywords:
HWENO method
Hamilton–Jacobi equation
Finite volume method
Monotone modification

ABSTRACT

In this paper, we present a class of new Hermite weighted essentially non-oscillatory (HWENO) schemes based on finite volume framework to directly solve the Hamilton–Jacobi (HJ) equations. For HWENO reconstruction, both the cell average and the first moment of the solution are evolved, and for two dimensional case, HWENO reconstruction is based on a dimension-by-dimension strategy which is the first used in HWENO reconstruction. For spatial discretization, one of key points for directly solving HJ equation is the reconstruction of numerical fluxes. We follow the idea put forward by Cheng and Wang (2014) [3] to reconstruct the values of solution at Gauss–Lobatto quadrature points and numerical fluxes at the interfaces of cells, and for neither the convex nor concave Hamiltonian case, the monotone modification of numerical fluxes is added, which can guarantee the precision in the smooth region and converge to the entropy solution when derivative discontinuities come up. The third order TVD Runge–Kutta method is used for the time discretization. Extensive numerical experiments in one dimensional and two dimensional cases are performed to verify the efficiency of the methods.

1. Introduction

In this paper, we use the finite volume Hermite weighted essentially non-oscillatory (HWENO) method for directly solving the Hamilton–Jacobi (HJ) equation:

$$\phi_t + H(\nabla_{\mathbf{x}}\phi, \mathbf{x}) = 0, \quad \phi(\mathbf{x}, 0) = \phi_0(\mathbf{x}) \quad \mathbf{x} \in \Omega \subset \mathbb{R}^d$$

where $\nabla_{\mathbf{x}}\phi = (\phi_{x_1}, \phi_{x_2}, \ldots, \phi_{x_n})^T$.

The HJ equation arises from many applications, such as control theory, geometric optics, image processing, level set method and so on. It is well known that the solutions of the nonlinear HJ equation are typically continuous, and the derivatives would be discontinuous even though the initial condition $\phi_0(\mathbf{x})$ is smooth enough. After suitable assumption [4], we can obtain the generalized solution, namely the viscosity solution, and the existence and uniqueness can be held.

Many successful numerical schemes for conservation laws have been successfully developed for HJ equations. Now, we briefly review the early works. First, we would like to mention the Crandall and Lion [5], they introduced a class of the monotone schemes, and proved that the solutions of those schemes converge to the viscosity solution. Osher and

☆ The research was supported by NSFC grants 91230110, 11571290 and 91530107.
* Corresponding author.
E-mail addresses: fzbz200808-31@163.com (F. Zheng), jxqiu@xmu.edu.cn (J. Qiu).

http://dx.doi.org/10.1016/j.jcp.2015.12.011
0021-9991/

Sethian [11] developed a second order essentially non-oscillatory, termed ENO schemes, and later Osher and Shu [12] proposed high order ENO schemes. Further, Jiang and Peng [7] presented the high order Weighted ENO, termed WENO, which can refer to [19], scheme to solve the HJ equations. Qiu and his colleagues [15,13] developed Hermite WENO, termed HWENO, schemes for HJ equations with Runge–Kutta or Lax–Wendroff time discretization, the first HWENO was presented by Qiu and Shu [14], and also used as limiter procedure for discontinuous Galerkin (DG) method. The schemes designed above are in the structured mesh. There are also schemes solving the HJ equations on the unstructured mesh. Abgrall [1] proposed the monotone schemes on triangular meshes, good property as it is, unfortunately it is only one order. Lafon and Osher [9] designed the second order schemes, and high order WENO schemes are developed by Zhang and Shu [23]. For a detail review of high order HJ equations, we refer to the lecture notes [18].

We have mentioned the different methods in solving HJ equations, and each of them can achieve good performance. But many of the schemes are based on finite difference method instead of finite volume method which may be more preferable on unstructured meshes. Hu and Shu [6] proposed a DG method to solve the HJ equation. Later, Li and Shu [10] reinterpreted the method of Hu and Shu. These methods are based on the fact that the derivatives of the solution ϕ satisfy the conservation laws, which is correct in one dimensional case but only weakly hyperbolic in multi-dimensional case. What's more, since they should recover the solution ϕ from its derivatives, the methods appear to be complicated and indirect. Cheng and Shu [2] apply the DG method directly to the HJ equation. As to the variable coefficient linear equation, this method is equivalent to the traditional DG method for conservation laws with source term. Due to this property, the stability and the error estimate can be easily performed. Later, Yan and Osher [22] proposed the local DG (LDG) method to deal with HJ equation, and we can see that the method is the general extension of the monotone schemes. Recently, Cheng and Wang [3] also improved their early work by utilizing the Roe speed and entropy fix at the cell interface.

The new methods presented in this paper have some advantages. First, we use the HWENO method, the WENO and HWENO methods have the similar building block to solve the HJ equations. Both of them can achieve the high order accuracy and maintain the essentially non-oscillatory property, based on using the adaptive stencils. The major difference between the HWENO and the WENO method is that the former one need extra work and storage but it is much more compact than the latter one in the same accuracy, owing to using both the cell average and its first moment in the reconstruction and evolving both of them. Second, our schemes can directly solve the HJ equation. The HJ equations cannot be written in a "conservation form", they are hard to be solved by finite volume method. As the HJ equations are closely related to the conservation laws, the former are simply the integral version of the latter one in one dimensional case. Many methods designed for conservation laws can be easily developed for HJ equations. However, they are indirect and complicated. Our schemes can achieve the goal to solve the HJ equations directly by carefully designing the Hamiltonian flux which is developed in [3] and adding monotone modification in neither convex nor concave case which is able to keep the precision in smooth area and ensure the convergence when the derivatives discontinuity appear. Third, the HWENO reconstruction in two dimensional case is based on the dimension-by-dimension strategy, which is the first used in HWENO reconstruction. The dimension-by-dimension strategy of HWENO reconstruction can achieve the same essentially non-oscillatory property as the genuine two-dimensional strategy, and it is less expensive and easier to code than the latter one.

In this paper, we follow the idea to reconstruct numerical fluxes at the interfaces of cells by Cheng and Wang [3] which is designed in DG methods, and for neither the convex nor concave case the monotone modification is added. HWENO procedure is applied to reconstruct the values of solution at Gauss–Lobatto quadrature points and the interfaces of the cell, the reconstruction procedure is similar to that as limiter for DG methods in [14], and in two dimensional case, HWENO reconstruction is based on a dimension-by-dimension strategy. The third order TVD Runge–Kutta method [20] is used for the time discretization.

The paper is organized as follows. In Section 2, we describe in detail the reconstruction and implementation of the finite volume HWENO schemes in one dimension and two dimension for directly solving the HJ equations. In Section 3, we present extensive numerical results to verify the accuracy and the stability of the method. Finally, a conclusion is given in Section 4.

2. The numerical method for the Hamilton–Jacobi equations

In this section, we will design the numerical method for both one and two dimensional Hamilton–Jacobi equations.

2.1. One dimensional Hamilton–Jacobi equations

The Hamilton–Jacobi equations in one dimensional case can be written as:

$$\phi_t + H(\phi_x, x) = 0 \qquad \phi(x,0) = \phi_0(x). \tag{2.1}$$

For simplicity, we assume the computational domain has been uniformly divided into cells $I_j = [x_{j-\frac{1}{2}}, x_{j+\frac{1}{2}}]$, $j = 1, \cdots, N$. The cell center and the mesh size is denoted as $x_j = (x_{j-\frac{1}{2}} + x_{j+\frac{1}{2}})/2$ and $\Delta x = x_{j+\frac{1}{2}} - x_{j-\frac{1}{2}}$. Furthermore, we define

$$U_j = \frac{1}{\Delta x}\int_{I_j} \phi(x,t)dx, \qquad V_j = \frac{1}{\Delta x}\int_{I_j} \phi(x,t)\frac{x - x_j}{\Delta x}dx$$

as the numerical approximate to the viscosity solution and its first moment of (2.1). We multiply (2.1) by 1 and $\frac{x-x_j}{\Delta x}$ and integrate them on cell I_j, respectively, then we have:

$$\begin{cases} \dfrac{dU_j}{dt} = -\dfrac{1}{\Delta x}\displaystyle\int_{I_j} H(\phi_x, x)dx \\ \dfrac{dV_j}{dt} = -\dfrac{1}{\Delta x}\displaystyle\int_{I_j} H(\phi_x, x)\dfrac{x-x_j}{\Delta x}dx \end{cases} \tag{2.2}$$

The integrals in (2.2) are computed by four point Gauss–Lobatto quadrature formula, respectively. For stability, following the directly solving HJ equation by discontinuous Galerkin (DG) method which was developed by Cheng and Wang [3], we add penalty terms for numerical fluxes at the interfaces of computational cells, and we have the following schemes:

$$\begin{aligned} \frac{dU_j}{dt} &= -\frac{1}{\Delta x}(\Delta x\sum_{G_l}\omega_l H(\phi_x, G_l) + \min(\widetilde{H}_\phi(x_{j+\frac{1}{2}}), 0)[\phi]_{j+\frac{1}{2}} + \max(\widetilde{H}_\phi(x_{j-\frac{1}{2}}), 0)[\phi]_{j-\frac{1}{2}}) \\ &\quad + C(S_\phi(x_{j+\frac{1}{2}}) - |\widetilde{H}_\phi(x_{j+\frac{1}{2}})|)[\phi_x]_{j+\frac{1}{2}} + C(S_\phi(x_{j-\frac{1}{2}}) - |\widetilde{H}_\phi(x_{j-\frac{1}{2}})|)[\phi_x]_{j-\frac{1}{2}} \\ \frac{dV_j}{dt} &= -\frac{1}{\Delta x}(\Delta x\sum_{G_l}\omega_l G_l H(\phi_x, G_l) + \frac{1}{2}\min(\widetilde{H}_\phi(x_{j+\frac{1}{2}}), 0)[\phi]_{j+\frac{1}{2}} \\ &\quad - \frac{1}{2}\max(\widetilde{H}_\phi(x_{j-\frac{1}{2}}), 0)[\phi]_{j-\frac{1}{2}}) \\ &\quad + \frac{1}{2}C(S_\phi(x_{j+\frac{1}{2}}) - |\widetilde{H}_\phi(x_{j+\frac{1}{2}})|)[\phi_x]_{j+\frac{1}{2}} - \frac{1}{2}C(S_\phi(x_{j-\frac{1}{2}}) - |\widetilde{H}_\phi(x_{j-\frac{1}{2}})|)[\phi_x]_{j-\frac{1}{2}} \end{aligned} \tag{2.3}$$

where G_l, ω_l are Gauss–Lobatto quadrature points and coefficients, respectively,

$$\begin{aligned} &G_1 = x_{j-\frac{1}{2}}, \quad G_2 = x_{j-\frac{\sqrt{5}}{10}}, \quad G_3 = x_{j+\frac{\sqrt{5}}{10}}, \quad G_4 = x_{j+\frac{1}{2}} \\ &\omega_1 = \frac{1}{12}, \quad \omega_2 = \frac{5}{12}, \quad \omega_3 = \frac{5}{12}, \quad \omega_4 = \frac{1}{12}, \end{aligned}$$

and $[u] = u^+ - u^-$ denotes the jump of u at the cell interface, and the superscripts $+$, $-$ denote the right, and left limits of a function. C is a positive penalty parameter taken as 0.25, $\widetilde{H}_\phi$ and S_ϕ are the Roe speed and the parameter to identify the entropy violating cells, which are defined as following, respectively.

$$\widetilde{H}_\phi(x_{j\pm\frac{1}{2}}) = \begin{cases} \dfrac{H(\phi_x(x^+_{j\pm\frac{1}{2}}), x^+_{j\pm\frac{1}{2}}) - H(\phi_x(x^-_{j\pm\frac{1}{2}}), x^-_{j\pm\frac{1}{2}})}{\phi_x(x^+_{j\pm\frac{1}{2}}) - \phi_x(x^-_{j\pm\frac{1}{2}})}, & \phi_x(x^+_{j\pm\frac{1}{2}}) \neq \phi_x(x^-_{j\pm\frac{1}{2}}) \\ \dfrac{1}{2}H_1(\phi_x(x^+_{j\pm\frac{1}{2}}), x^+_{j\pm\frac{1}{2}}) + \dfrac{1}{2}H_1(\phi_x(x^-_{j\pm\frac{1}{2}}), x^-_{j\pm\frac{1}{2}}), & \phi_x(x^+_{j\pm\frac{1}{2}}) = \phi_x(x^-_{j\pm\frac{1}{2}}), \end{cases}$$

$$\delta_\phi(x_{j\pm\frac{1}{2}}) = \max(0, \widetilde{H}_\phi(x_{j\pm\frac{1}{2}}) - H_1(\phi_x(x^-_{j\pm\frac{1}{2}}), x^-_{j\pm\frac{1}{2}}), H_1(\phi_x(x^+_{j\pm\frac{1}{2}}), x^+_{j\pm\frac{1}{2}}) - \widetilde{H}_\phi(x_{j\pm\frac{1}{2}}))$$

and

$$S_\phi(x_{j\pm\frac{1}{2}}) = \max(\delta_\phi(x_{j\pm\frac{1}{2}}), |\widetilde{H}_\phi(x_{j\pm\frac{1}{2}})|),$$

where $H_1 = \partial H/\partial\phi_x$ is the partial derivative of Hamiltonian with respect to ϕ_x.

The values of ϕ and ϕ_x at the Gauss–Lobatto points and the cell interface will be reconstructed by fifth order HWENO method, which will be described in subsection 2.2. Then, we can rewrite the schemes as $U_t = \mathcal{L}(U)$, where the $\mathcal{L}$ denotes the operator of spatial discretization, and use the third-order total variation diminishing (TVD) Runge–Kutta time discretization [20] to solve the semi-discrete form (2.3):

$$\begin{cases} U^{(1)} = U^n + \Delta t\mathcal{L}(U^n) \\ U^{(2)} = \dfrac{3}{4}U^n + \dfrac{1}{4}(U^{(1)} + \Delta t\mathcal{L}(U^{(1)})) \\ U^{n+1} = \dfrac{1}{3}U^n + \dfrac{2}{3}(U^{(2)} + \Delta t\mathcal{L}(U^{(2)})) \end{cases} \tag{2.4}$$

2.2. HWENO reconstruction in one dimensional case

In this subsection, we will describe the HWENO reconstruction procedure for the $\phi^{\pm}_{j+\frac{1}{2}}$, $\phi^{\pm}_{j-\frac{1}{2}}$, $\phi_x{}^{\pm}_{j+\frac{1}{2}}$, $\phi_x{}^{\pm}_{j-\frac{1}{2}}$ and $\phi_{x_{j\pm\frac{\sqrt{5}}{10}}}$.

Step 1. Reconstruction of $\phi^{\mp}_{j\pm\frac{1}{2}}$ by HWENO method from the cell averages $\{U_j, V_j\}$

1.1. Given the small stencils $S_0=\{I_{j-1}, I_j\}$, $S_1=\{I_j, I_{j+1}\}$, $S_2=\{I_{j-1}, I_j, I_{j+1}\}$, and the bigger stencils $\mathcal{T}=\{S_0, S_1, S_2\}$, we construct Hermite cubic polynomials $p_0(x)$, $p_1(x)$, $p_2(x)$, and a fifth-degree polynomial $q(x)$ such that:

$$\frac{1}{\Delta x}\int_{I_{i+j}} p_0(x)dx = U_{i+j}, \qquad \frac{1}{\Delta x}\int_{I_{i+j}} p_0(x)\frac{x-x_{i+j}}{\Delta x}dx = V_{i+j}, \quad i=-1,0, \tag{2.5}$$

$$\frac{1}{\Delta x}\int_{I_{i+j}} p_1(x)dx = U_{i+j}, \qquad \frac{1}{\Delta x}\int_{I_{i+j}} p_1(x)\frac{x-x_{i+j}}{\Delta x}dx = V_{i+j}, \quad i=0,1, \tag{2.6}$$

$$\frac{1}{\Delta x}\int_{I_{i+j}} p_2(x)dx = U_{i+j}, \qquad \frac{1}{\Delta x}\int_{I_j} p_2(x)\frac{x-x_j}{\Delta x}dx = V_j, \quad i=-1,0,1, \tag{2.7}$$

$$\frac{1}{\Delta x}\int_{I_{i+j}} q(x)dx = U_{i+j}, \qquad \frac{1}{\Delta x}\int_{I_{i+j}} q(x)\frac{x-x_{i+j}}{\Delta x}dx = V_{i+j}, \quad i=-1,0,1, \tag{2.8}$$

we only need the values of these polynomials at the boundary $x^{\mp}_{j\pm\frac{1}{2}}$, which have the following expressions:

$$p_0(x^-_{j+\frac{1}{2}}) = \frac{3}{4}U_{j-1}+\frac{1}{4}U_j+\frac{7}{2}V_{j-1}+\frac{23}{2}V_j$$
$$p_1(x^-_{j+\frac{1}{2}}) = \frac{1}{2}U_j+\frac{1}{2}U_{j+1}+2V_j-2V_{j+1}$$
$$p_2(x^-_{j+\frac{1}{2}}) = \frac{2}{33}U_{j-1}+\frac{5}{6}U_j+\frac{7}{66}U_{j+1}+\frac{60}{11}V_j$$
$$q(x^-_{j+\frac{1}{2}}) = \frac{13}{108}U_{j-1}+\frac{7}{12}U_j+\frac{8}{27}U_{j+1}+\frac{25}{54}V_{j-1}+\frac{241}{54}V_j-\frac{28}{27}V_{j+1}$$
$$p_0(x^+_{j-\frac{1}{2}}) = \frac{1}{2}U_{j-1}+\frac{1}{2}U_j+2V_{j-1}-2V_j$$
$$p_1(x^+_{j-\frac{1}{2}}) = \frac{1}{4}U_j+\frac{3}{4}U_{j+1}-\frac{23}{2}V_j-\frac{7}{2}V_{j+1}$$
$$p_2(x^+_{j-\frac{1}{2}}) = \frac{7}{66}U_{j-1}+\frac{5}{6}U_j+\frac{2}{33}U_{j+1}-\frac{60}{11}V_j$$
$$q(x^+_{j-\frac{1}{2}}) = \frac{8}{27}U_{j-1}+\frac{7}{12}U_j+\frac{13}{108}U_{j+1}+\frac{28}{27}V_{j-1}-\frac{241}{54}V_j-\frac{25}{54}V_{j+1}$$

1.2. For each small stencils S_m, $m=0,1,2$, we compute the smooth indicators respectively, which measure the smoothness of the reconstructed polynomials $p_m(x)$, $m=0,1,2$ in the target cell I_j. The smaller the indicator is, the smoother the polynomial is in the target cells. We define the smooth indicators as in [8]:

$$\beta_m = \sum_{l=1}^{3}\int_{I_j} \Delta x^{2l-1}\left(\frac{\partial^l}{\partial x^l}p_m(x)\right)^2 dx \qquad m=0,1,2 \tag{2.9}$$

1.3. We compute the linear weights, denoted by $\gamma_m(x^{\mp}_{j\pm\frac{1}{2}})$, $m=0,1,2$, satisfying:

$$q(x^{\mp}_{j\pm\frac{1}{2}}) = \sum_{m=0}^{2}\gamma_m(x^{\mp}_{j\pm\frac{1}{2}})p_m(x^{\mp}_{j\pm\frac{1}{2}})$$

for all the cell averages of $\{U_j\}$ and $\{V_j\}$ in the bigger stencils $\mathcal{T}$, which leads to

$$\gamma_0(x^-_{j+\frac{1}{2}}) = \frac{25}{189}, \qquad \gamma_1(x^-_{j+\frac{1}{2}}) = \frac{14}{27}, \qquad \gamma_2(x^-_{j+\frac{1}{2}}) = \frac{22}{63}$$
$$\gamma_0(x^+_{j-\frac{1}{2}}) = \frac{14}{27}, \qquad \gamma_1(x^+_{j-\frac{1}{2}}) = \frac{25}{189}, \qquad \gamma_2(x^+_{j-\frac{1}{2}}) = \frac{22}{63}$$

1.4. We compute the nonlinear weights based on the linear weights and the smooth indicators by:

$$\omega_m(x^{\mp}_{j\pm\frac{1}{2}}) = \frac{\overline{\omega_m}(x^{\mp}_{j\pm\frac{1}{2}})}{\sum_k \overline{\omega_k}(x^{\mp}_{j\pm\frac{1}{2}})} \qquad \overline{\omega_m}(x^{\mp}_{j\pm\frac{1}{2}}) = \frac{\gamma_m(x^{\mp}_{j\pm\frac{1}{2}})}{(\beta_m+\varepsilon)^2} \qquad m=0,1,2 \tag{2.10}$$

where the ε is a small positive number to avoid the denominator becoming zero. In our paper, we use $\varepsilon = 10^{-6}$. The final HWENO approximation expression is:

$$\phi^{\mp}_{j\pm\frac{1}{2}} \approx \sum_{m=0}^{2} \omega_m(x^{\mp}_{j\pm\frac{1}{2}}) p_m(x^{\mp}_{j\pm\frac{1}{2}}),$$

Step 2. Reconstruction of $\{\phi_{x^{\mp}_{j\pm\frac{1}{2}}}\}$ and $\{\phi_{x_{j\pm\frac{\sqrt{5}}{10}}}\}$ by fifth order HWENO from the cell average $\{U_j, V_j\}$

2.1. Given the small stencils $S_0=\{I_{j-1}, I_j\}$, $S_1=\{I_j, I_{j+1}\}$, $S_2=\{I_{j-1}, I_j, I_{j+1}\}$, and the bigger stencils $\mathcal{T}=\{S_0, S_1, S_2\}$, we construct Hermite cubic reconstruction polynomials $p_0(x)$, $p_1(x)$, $p_2(x)$, and a fifth-degree reconstruction polynomial $q(x)$, such that the polynomials satisfy the conditions (2.5), (2.6), (2.7), (2.8). We need the derivative values of these polynomials at the four Gauss–Lobatto quadrature points $x^{-}_{j+\frac{1}{2}}$, $x_{j+\frac{\sqrt{5}}{10}}$, $x_{j-\frac{\sqrt{5}}{10}}$ and $x^{+}_{j-\frac{1}{2}}$ denoted as G_1, G_2, G_3, G_4 respectively, which have the following polynomial expressions:

$$\begin{aligned}
p_0'(x) &= \frac{1}{\Delta x}[-\frac{3}{8}U_{j-1}+\frac{3}{8}U_j-\frac{9}{4}V_{j-1}+\frac{39}{4}V_j+(\frac{15}{2}U_{j-1}-\frac{15}{2}U_j+33V_{j-1}+57V_j)(\frac{x-x_j}{\Delta x})\\
&\quad+(\frac{15}{2}U_{j-1}-\frac{15}{2}U_j+45V_{j-1}+45V_j)(\frac{x-x_j}{\Delta x})^2],\\
p_1'(x) &= \frac{1}{\Delta x}[-\frac{3}{8}U_j+\frac{3}{8}U_{j+1}+\frac{39}{4}V_j-\frac{9}{4}V_{j+1}+(-\frac{15}{2}U_j+\frac{15}{2}U_{j+1}-57V_j-33V_{j+1})(\frac{x-x_j}{\Delta x})\\
&\quad+(\frac{15}{2}U_j-\frac{15}{2}U_{j+1}+45V_j+45V_{j+1})(\frac{x-x_j}{\Delta x})^2],\\
p_2'(x) &= \frac{1}{\Delta x}[\frac{3}{44}U_{j-1}-\frac{3}{44}U_{j+1}+\frac{150}{11}V_j+(U_{j-1}-2U_j+U_{j+1})(\frac{x-x_j}{\Delta x})\\
&\quad+(-\frac{15}{11}U_{j-1}+\frac{15}{11}U_{j+1}-\frac{360}{11}V_j)(\frac{x-x_j}{\Delta x})^2],\\
q'(x) &= \frac{1}{\Delta x}[(\frac{167}{576}U_{j-1}-\frac{167}{576}U_{j+1}+\frac{281}{288}V_{j-1}+\frac{2449}{144}V_j+\frac{281}{288}V_{j+1})\\
&\quad+(\frac{23}{8}U_{j-1}-\frac{23}{4}U_j+\frac{23}{8}U_{j+1}+\frac{45}{4}V_{j-1}-\frac{45}{4}V_{j+1})(\frac{x-x_j}{\Delta x})\\
&\quad+(-\frac{455}{72}U_{j-1}+\frac{455}{72}U_{j+1}-\frac{785}{36}V_{j-1}-\frac{1945}{18}V_j-\frac{785}{36}V_{j+1})(\frac{x-x_j}{\Delta x})^2\\
&\quad+(-\frac{5}{2}U_{j-1}+5U_j-\frac{5}{2}U_{j+1}-15V_{j-1}+15V_{j+1})(\frac{x-x_j}{\Delta x})^3\\
&\quad+(\frac{175}{36}U_{j-1}-\frac{175}{36}U_{j+1}+\frac{385}{18}V_{j-1}+\frac{665}{9}V_j+\frac{385}{18}V_{j+1})(\frac{x-x_j}{\Delta x})^4].
\end{aligned}$$

2.2. We define the smooth indicators as in [8]:

$$\beta_m = \sum_{l=2}^{3}\int_{I_j} \Delta x^{2l-1}(\frac{\partial^l p_m(x)}{\partial x^l})^2 dx, \qquad m=0,1,2 \tag{2.11}$$

2.3. We compute the linear weights, denoted by $\gamma_m(G_l)$, $l=1,2,3,4$, such that:

$$q'(G_l) = \sum_{m=0}^{2} \gamma_m(G_l) p_m'(G_l), \qquad l=1,2,3,4,$$

for all the cell averages of $\{U_j\}$ and $\{V_j\}$ in the bigger stencils $\mathcal{T}$, which leads to

$$\begin{aligned}
&\gamma_0(G_1)=\frac{11}{459}, && \gamma_1(G_1)=\frac{124}{135}, && \gamma_2(G_1)=\frac{44}{765}\\
&\gamma_0(G_2)=-\frac{1}{54\sqrt{5}}+\frac{7}{22}, && \gamma_1(G_2)=\frac{1}{54\sqrt{5}}+\frac{7}{22}, && \gamma_2(G_2)=\frac{4}{11}
\end{aligned}$$

$$\gamma_0(G_3)=\frac{1}{54\sqrt{5}}+\frac{7}{22},\qquad \gamma_1(G_3)=-\frac{1}{54\sqrt{5}}+\frac{7}{22},\qquad \gamma_2(G_3)=\frac{4}{11}$$
$$\gamma_0(G_4)=\frac{124}{135},\qquad \gamma_1(G_4)=\frac{11}{459},\qquad \gamma_2(G_4)=\frac{44}{765}$$

2.4. We compute the nonlinear weights by (2.10). The final HWENO approximation expressions are:

$$\phi_x(G_l)\approx\sum_{m=0}^{2}\omega_m(G_l)p'_m(G_l),\qquad l=1,2,3,4,$$

respectively.

If H is a neither convex nor concave Hamiltonian, our method would not necessarily converge to the unique entropy solution. Inspired by [16], we also add the extra monotone modification into each Runge–Kutta step, which can help our method converge to the viscosity solution in general neither convex nor concave case and maintain the high order in smooth regions.

Before modify our method, we should design the discontinuity indicator on cell I_j, termed φ_j. Here we recommend the indicator [21], which is defined as follows:

$$\varphi_j=\frac{\beta_j}{\beta_j+\gamma_j}$$

where

$$\alpha_j=|W_{j-1}-W_j|^2+\varepsilon\quad \xi_j=|W_{j-1}-W_{j+1}|^2+\varepsilon$$
$$\beta_j=\frac{\xi_j}{\alpha_{j-1}}+\frac{\xi_j}{\alpha_{j+2}},\qquad \gamma_j=M(\frac{|W_{\max}-W_{\min}|^2}{\alpha_j}+\frac{|W_{\max}-W_{\min}|^2}{\alpha_{j+1}})$$

Here, W_j denotes the cell average of the derivative of the solution ϕ on I_j, which is computed by Gauss–Lobatto quadrature formula numerically, and $\varepsilon=10^{-6}$ in order to avoid the denominator becoming zero. $W_{\max}$ and $W_{\min}$ are the maximum and minimum of W_j respectively. M is a discontinuity parameter, and we hereby choose $M=10000$. The discontinuity indicator φ_j has the properties: (a). $0\le\varphi_j\le 1$; (b). φ_j is $O(\Delta x^2)$ in smooth region; (c). φ_j close to $O(1)$ near the derivative discontinuity. Now we modify our method by following steps for one dimensional method:

(1) Identify the troubled cell in which the Hamiltonian $H(u)$ is neither convex nor concave. We call cell I_j a good cell if $\phi^{\pm}_{j-\frac{1}{2}}$ and $\phi^{\pm}_{j+\frac{1}{2}}$ all fall into the same convex or concave region of the Hamiltonian $H(u)$, otherwise we define the cell as a troubled cell [16].

(2) When I_j is identified as a troubled cell, the solution U_j^{n+1} will be modified by following method.

(a). Define $U_j^{n+1_{mono}}$ by:

$$U_j^{n+1_{mono}}=U_j^n-\Delta t(H(\frac{U_{j+1}^n-U_{j-1}^n}{2\Delta x})-\frac{1}{2}\alpha(\frac{U_{j+1}^n-2U_j^n+U_{j-1}^n}{\Delta x})) \tag{2.12}$$

with $\alpha=\max_u|H'(u)|$.

(b). Modify U_j^{n+1} by combination of U_j^{n+1} and $U_j^{n+1_{mono}}$:

$$U_j^{n+1_{mod}}=(1-\varphi_j^2)U_j^{n+1}+\varphi_j^2U_j^{n+1_{mono}} \tag{2.13}$$

The advantage of the method we design above is the self-adaptive: if the derivative of the solution is with a strong discontinuity, φ_j is close to $O(1)$, then the monotone scheme comes into effect; if the derivative of the solution is in a smooth area, φ_j is close to $O(\Delta x^2)$; what's more, $0\le\phi_j\le 1$. We denote (2.3) as $U_j^{n+1}=U_j^n+\Delta t\mathbb{L}_1(U)$ and denote (2.12) as $U_j^{n+1}=U_j^n+\Delta t\mathbb{L}_2(U)$, so we can rewrite (2.13) as

$$U_j^{n+1_{mod}}=U_j^n+\Delta t(1-\varphi_j^2)\mathbb{L}_1(U)+\Delta t\varphi_j^2\mathbb{L}_2(U).$$

For space discretization $\mathbb{L}_1(U)$ is fifth order approximation to $H(u)$ and the $\mathbb{L}_2(U)$ is the first order approximation to $H(u)$, so in the smooth region of solution, we have:

$$\varphi_j^2|\mathbb{L}_1(U)-\mathbb{L}_2(U)|\sim O(\Delta x^5),$$

that is, the modification does not change the accurate of the schemes, and after modified procedure, we denote $U_j^{n+1_{mod}}$ as U_j^{n+1}.

(3) If U_j^{n+1} is modified, then we will modify V_j^{n+1} by Step 3.

Step 3. Reconstruction of $V_j^{n+1_{mod}}$ by fifth order HWENO from the cell average $\{U_j^{n+1}, V_j^{n+1}\}$

3.1. Given the small stencils $S_0 = \{I_{j-1}, I_j\}$, $S_1 = \{I_j, I_{j+1}\}$, $S_2 = \{I_{j-1}, I_j, I_{j+1}\}$ and the bigger stencils $\mathcal{T} = \{S_0, S_1, S_2\}$, we construct Hermite quadratic reconstruction polynomials $p_0(x)$, $p_1(x)$, $p_2(x)$, and a quartic reconstruction polynomial $q(x)$ respectively, such that the polynomials satisfy the conditions.

$$\begin{aligned}
&\frac{1}{\Delta x}\int_{I_{i+j}} p_0(x)dx = U_{i+j}^{n+1}, \quad \frac{1}{\Delta x}\int_{I_{j-1}} p_0(x)\frac{x-x_{j-1}}{\Delta x}dx = V_{j-1}^{n+1}, \quad i=-1,0\\
&\frac{1}{\Delta x}\int_{I_{i+j}} p_1(x)dx = U_{i+j}^{n+1}, \quad \frac{1}{\Delta x}\int_{I_{j+1}} p_1(x)\frac{x-x_{j+1}}{\Delta x}dx = V_{j+1}^{n+1}, \quad i=0,1\\
&\frac{1}{\Delta x}\int_{I_{i+j}} p_2(x)dx = U_{i+j}^{n+1}, \qquad\qquad\qquad\qquad\qquad\qquad\quad i=-1,0,1.\\
&\frac{1}{\Delta x}\int_{I_{i+j}} q(x)dx = U_{i+j}^{n+1}, \quad \frac{1}{\Delta x}\int_{I_{j\pm1}} q(x)\frac{x-x_{j\pm1}}{\Delta x}dx = V_{j\pm1}^{n+1}, \quad i=-1,0,1
\end{aligned}$$

We only need the first moment of these polynomials in the cell I_j, which have the following polynomial expressions:

$$\begin{aligned}
&\frac{1}{\Delta x}\int_{I_j} p_0(x)\frac{x-x_j}{\Delta x}dx = -\frac{1}{6}U_{j-1}^{n+1} + \frac{1}{6}U_j^{n+1} - V_{j-1}^{n+1},\\
&\frac{1}{\Delta x}\int_{I_j} p_1(x)\frac{x-x_j}{\Delta x}dx = \frac{1}{6}U_{j+1}^{n+1} - \frac{1}{6}U_j^{n+1} - V_{j+1}^{n+1},\\
&\frac{1}{\Delta x}\int_{I_j} p_2(x)\frac{x-x_j}{\Delta x}dx = \frac{1}{24}U_{j+1}^{n+1} - \frac{1}{24}U_{j-1}^{n+1},\\
&\frac{1}{\Delta x}\int_{I_j} q(x)\frac{x-x_j}{\Delta x}dx = -\frac{5}{76}U_{j-1}^{n+1} + \frac{5}{76}U_{j+1}^{n+1} - \frac{11}{38}V_{j-1}^{n+1} - \frac{11}{38}V_{j+1}^{n+1}.
\end{aligned} \tag{2.14}$$

3.2. We define the smooth indicator as in [8]:

$$\beta_m = \sum_{l=1}^{2}\int_{I_j} \Delta x^{2l-1}\left(\frac{\partial^l p_m(x)}{\partial x^l}\right)^2 dx \qquad m=0,1,2.$$

3.3. We compute the linear weights, denoted by $\gamma_m, m=0,1,2$, satisfying:

$$\frac{1}{\Delta x}\int_{I_j} q(x)\frac{x-x_j}{\Delta x}dx = \sum_{m=0}^{2}\gamma_m\frac{1}{\Delta x}\int_{I_j} p_m(x)\frac{x-x_j}{\Delta x}dx,$$

for all the cell averages of $\{U_j^{n+1}\}$ and $\{V_j^{n+1}\}$ in the bigger stencils $\mathcal{T}$, which leads to

$$\gamma_0 = \frac{11}{38}, \quad \gamma_1 = \frac{11}{38}, \quad \gamma_2 = \frac{8}{19}.$$

3.4. We compute the nonlinear weights as (2.10), and the $V_j^{n+1_{mod}}$ approximation expression is:

$$V_j^{n+1_{mod}} = \sum_{m=0}^{2}\omega_m\frac{1}{\Delta x}\int_{I_j} p_m(x)\frac{x-x_j}{\Delta x}dx.$$

3.5. We denote $V_j^{n+1_{mod}}$ as V_j^{n+1}.

2.3. Two dimensional Hamilton–Jacobi equations

The Hamilton–Jacobi equations in two dimensional case are written as

$$\phi_t + H(\phi_x, \phi_y, x, y) = 0 \qquad \phi(x,y,0) = \phi_0(x,y) \tag{2.15}$$

for simplicity, we also assume the computational domain has been uniformly divided into cells $I_{ij} = [x_{i-\frac{1}{2}}, x_{i+\frac{1}{2}}] \times [y_{j-\frac{1}{2}}, y_{j+\frac{1}{2}}]$, $J_i = [x_{i-\frac{1}{2}}, x_{i+\frac{1}{2}}]$, $K_j = [y_{j-\frac{1}{2}}, y_{j+\frac{1}{2}}]$, $i = 1, \cdots, N$, $j = 1, \cdots, N$. We also denote the cell center as $(x_i, y_j) = ((x_{i-\frac{1}{2}} + x_{i+\frac{1}{2}})/2, (y_{j-\frac{1}{2}} + y_{j+\frac{1}{2}})/2)$, and the mesh size as $\Delta x = x_{i+\frac{1}{2}} - x_{i-\frac{1}{2}}$, $\Delta y = y_{j+\frac{1}{2}} - y_{j-\frac{1}{2}}$. Furthermore, we define

$$U_{i,j} = \frac{1}{\Delta x \Delta y} \iint_{I_{i,j}} \phi(x, y, t) dxdy, \qquad V_{i,j} = \frac{1}{\Delta x \Delta y} \iint_{I_{i,j}} \phi(x, y, t) \frac{x - x_i}{\Delta x} dxdy,$$

$$W_{i,j} = \frac{1}{\Delta x \Delta y} \iint_{I_{i,j}} \phi(x, y, t) \frac{y - y_j}{\Delta y} dxdy, \qquad T_{i,j} = \frac{1}{\Delta x \Delta y} \iint_{I_{i,j}} \phi(x, y, t) \frac{x - x_i}{\Delta x} \frac{y - y_j}{\Delta y} dxdy.$$

Multiply (2.15) by $v(x, y)$, which is equal to 1, $\frac{x-x_i}{\Delta x}$, $\frac{y-y_j}{\Delta y}$ and $\frac{x-x_i}{\Delta x}\frac{y-y_j}{\Delta y}$ respectively, and integrate them on cell $I_{i,j}$, respectively, then we have:

$$\begin{cases} \dfrac{dU_{i,j}}{dt} = -\dfrac{1}{\Delta x \Delta y} \iint_{I_{i,j}} H(\phi_x, \phi_y, x, y) dxdy, \\ \dfrac{dV_{i,j}}{dt} = -\dfrac{1}{\Delta x \Delta y} \iint_{I_{i,j}} H(\phi_x, \phi_y, x, y) \dfrac{x - x_i}{\Delta x} dxdy, \\ \dfrac{dW_{i,j}}{dt} = -\dfrac{1}{\Delta x \Delta y} \iint_{I_{i,j}} H(\phi_x, \phi_y, x, y) \dfrac{y - y_j}{\Delta y} dxdy, \\ \dfrac{dT_{i,j}}{dt} = -\dfrac{1}{\Delta x \Delta y} \iint_{I_{i,j}} H(\phi_x, \phi_y, x, y) \dfrac{x - x_i}{\Delta x} \dfrac{y - y_j}{\Delta y} dxdy. \end{cases} \tag{2.16}$$

The integrals (2.16) are computed by 16 points Gauss–Lobatto quadrature formula respectively. For stability, resorting to the method developed by Cheng and Wang [3], we also add penalty terms for numerical fluxes at the interfaces of computational cells, and we have the following schemes:

$$\begin{aligned} &\frac{d}{dt}\left(\frac{1}{\Delta x \Delta y} \iint_{I_{i,j}} \phi(x, y, t) v(x, y) dxdy\right) \\ &= -\sum_{l,k} \omega_l \omega_k H(\phi(xG_l, yG_k, t)_x, \phi(xG_l, yG_k, t)_y, xG_l, yG_k) v(xG_l, yG_k) \\ &\quad - \frac{1}{\Delta x} \sum_k \omega_k \min(\widetilde{H}_{1,\phi}(x_{i+\frac{1}{2}}, yG_k), 0)[\phi](x_{i+\frac{1}{2}}, yG_k) v(x^-_{i+\frac{1}{2}}, yG_k) \\ &\quad - \frac{1}{\Delta x} \sum_k \omega_k \max(\widetilde{H}_{1,\phi}(x_{i-\frac{1}{2}}, yG_k), 0)[\phi](x_{i-\frac{1}{2}}, yG_k) v(x^+_{i-\frac{1}{2}}, yG_k) \\ &\quad - \frac{1}{\Delta y} \sum_l \omega_l \min(\widetilde{H}_{2,\phi}(xG_l, y_{j+\frac{1}{2}}), 0)[\phi](xG_l, y_{j+\frac{1}{2}}) v(xG_l, y^-_{j+\frac{1}{2}}) \\ &\quad - \frac{1}{\Delta y} \sum_l \omega_l \max(\widetilde{H}_{2,\phi}(xG_l, y_{j-\frac{1}{2}}), 0)[\phi](xG_l, y_{j-\frac{1}{2}}) v(xG_l, y^+_{j-\frac{1}{2}}) \\ &\quad + C \sum_k \omega_k (S_{1,\phi}(x_{i+\frac{1}{2}}, yG_k) - |\widetilde{H}_{1,\phi}(x_{i+\frac{1}{2}}, yG_k)|)[\phi_x](x_{i+\frac{1}{2}}, yG_k) v(x^-_{i+\frac{1}{2}}, yG_k) \\ &\quad + C \sum_k \omega_k (S_{1,\phi}(x_{i-\frac{1}{2}}, yG_k) - |\widetilde{H}_{1,\phi}(x_{i-\frac{1}{2}}, yG_k)|)[\phi_x](x_{i-\frac{1}{2}}, yG_k) v(x^+_{i-\frac{1}{2}}, yG_k) \\ &\quad + C \sum_l \omega_l (S_{2,\phi}(xG_l, y_{j+\frac{1}{2}}) - |\widetilde{H}_{2,\phi}(xG_l, y_{j+\frac{1}{2}})|)[\phi_y](xG_l, y_{j+\frac{1}{2}}) v(xG_l, y^-_{j+\frac{1}{2}}) \\ &\quad + C \sum_l \omega_l (S_{2,\phi}(xG_l, y_{j-\frac{1}{2}}) - |\widetilde{H}_{2,\phi}(xG_l, y_{j-\frac{1}{2}})|)[\phi_y](xG_l, y_{j-\frac{1}{2}}) v(xG_l, y^+_{j-\frac{1}{2}}) \end{aligned} \tag{2.17}$$

where $v(x, y)$ refers to 1, $\frac{x-x_i}{\Delta x}$, $\frac{y-y_j}{\Delta y}$ and $\frac{x-x_i}{\Delta x}\frac{y-y_j}{\Delta y}$. xG_l, yG_k, ω_l, ω_k are the Gauss–Lobatto quadrature points and weights in x and y direction respectively:

$$xG_1 = x_{i-\frac{1}{2}}, \quad xG_2 = x_{i-\frac{\sqrt{5}}{10}}, \quad xG_3 = x_{i+\frac{\sqrt{5}}{10}}, \quad xG_4 = x_{i+\frac{1}{2}}$$
$$yG_1 = y_{j-\frac{1}{2}}, \quad yG_2 = y_{j-\frac{\sqrt{5}}{10}}, \quad yG_3 = y_{j+\frac{\sqrt{5}}{10}}, \quad yG_4 = y_{j+\frac{1}{2}}$$
$$\omega_1 = \frac{1}{12}, \quad \omega_2 = \frac{5}{12}, \quad \omega_3 = \frac{5}{12}, \quad \omega_4 = \frac{1}{12}$$

The symbol $[u] = u^+ - u^-$ denotes the jump of u at the cell interface, and the superscripts $+$, $-$ denote the right and left or top and bottom limits of a function. C is a positive penalty parameter taken as 0.25 and $\widetilde{H}_{1,\phi}$ is the Roe speed in the x direction defined as follows:

$$\widetilde{H}_{1,\phi}(x_{i\pm\frac{1}{2}}, y) = \begin{cases} \frac{H(\phi_x(x^+_{i\pm\frac{1}{2}}, y), \overline{\phi_y}, x^+_{i\pm\frac{1}{2}}, y) - H(\phi_x(x^-_{i\pm\frac{1}{2}}, y), \overline{\phi_y}, x^-_{i\pm\frac{1}{2}}, y)}{\phi_x(x^+_{i\pm\frac{1}{2}}, y) - \phi_x(x^-_{i\pm\frac{1}{2}}, y)}, & \phi_x(x^+_{i\pm\frac{1}{2}}, y) \neq \phi_x(x^-_{i\pm\frac{1}{2}}, y) \\ \frac{1}{2}H_1(\phi_x(x^+_{i\pm\frac{1}{2}}, y), \overline{\phi_y}, x^+_{i\pm\frac{1}{2}}, y) + \frac{1}{2}H_1(\phi_x(x^-_{i\pm\frac{1}{2}}, y), \overline{\phi_y}, x^-_{i\pm\frac{1}{2}}, y), & \phi_x(x^+_{i\pm\frac{1}{2}}, y) = \phi_x(x^-_{i\pm\frac{1}{2}}, y), \end{cases}$$

where, $H_1 = \partial H/\partial\phi_x$ refers to the partial derivative of Hamiltonian with respect to ϕ_x, and

$$\overline{\phi_y} = \frac{1}{2}(\phi_y(x^+_{i\pm\frac{1}{2}}, y) + \phi_y(x^-_{i\pm\frac{1}{2}}, y))$$

is the average of the tangential derivative.

$$\delta_{1,\phi}(x_{i\pm\frac{1}{2}}, y) = \max(0, \widetilde{H}_{1,\phi}(x_{i\pm\frac{1}{2}}, y) - H_1(\phi_x(x^-_{i\pm\frac{1}{2}}, y), \overline{\phi_y}, x^-_{i\pm\frac{1}{2}}, y), H_1(\phi_x(x^+_{i\pm\frac{1}{2}}, y), \overline{\phi_y}, x^+_{i\pm\frac{1}{2}}, y) - \widetilde{H}_{1,\phi}(x_{i\pm\frac{1}{2}}, y))$$

and

$$S_{1,\phi}(x_{i\pm\frac{1}{2}}, y) = \max(\delta_{1,\phi}(x_{i\pm\frac{1}{2}}, y), |\widetilde{H}_{1,\phi}(x_{i\pm\frac{1}{2}}, y)|)$$

are the arguments which are used to detect the entropy violating cells in the x direction.

Similarly, the Roe speed in the y direction defined as:

$$\widetilde{H}_{2,\phi}(x, y_{j\pm\frac{1}{2}}) = \begin{cases} \frac{H(\overline{\phi_x}, \phi_y(x, y^+_{j\pm\frac{1}{2}}), x, y^+_{j\pm\frac{1}{2}}) - H(\overline{\phi_x}, \phi_y(x, y^-_{j\pm\frac{1}{2}}), x, y^-_{j\pm\frac{1}{2}})}{\phi_y(x, y^+_{j\pm\frac{1}{2}}) - \phi_y(x, y^-_{j\pm\frac{1}{2}})}, & \phi_y(x, y^+_{j\pm\frac{1}{2}}) \neq \phi_y(x, y^-_{j\pm\frac{1}{2}}) \\ \frac{1}{2}H_2(\overline{\phi_x}, \phi_y(x, y^+_{j\pm\frac{1}{2}}), x, y^+_{j\pm\frac{1}{2}}) + \frac{1}{2}H_2(\overline{\phi_x}, \phi_y(x, y^-_{j\pm\frac{1}{2}}), x, y^-_{j\pm\frac{1}{2}}), & \phi_y(x, y^+_{j\pm\frac{1}{2}}) = \phi_y(x, y^-_{j\pm\frac{1}{2}}), \end{cases}$$

where, $H_2 = \partial H/\partial\phi_y$ refers to the partial derivative of Hamiltonian with respect to ϕ_y, and

$$\overline{\phi_x} = \frac{1}{2}(\phi_x(x, y^+_{j\pm\frac{1}{2}}) + \phi_x(x, y^-_{j\pm\frac{1}{2}}))$$

is the average of the tangential derivative.

$$\delta_{2,\phi}(x, y_{j\pm\frac{1}{2}}) = \max(0, \widetilde{H}_{2,\phi}(x, y_{j\pm\frac{1}{2}}) - H_2(\overline{\phi_x}, \phi_y(x, y^-_{j\pm\frac{1}{2}}), x, y^-_{j\pm\frac{1}{2}}), H_2(\overline{\phi_x}, \phi_y(x, y^+_{j\pm\frac{1}{2}}), x, y^+_{j\pm\frac{1}{2}}) - \widetilde{H}_{2,\phi}(x, y_{j\pm\frac{1}{2}}))$$

and

$$S_{2,\phi}(x, y_{j\pm\frac{1}{2}}) = \max(\delta_{2,\phi}(x, y_{j\pm\frac{1}{2}}), |\widetilde{H}_{2,\phi}(x, y_{j\pm\frac{1}{2}})|)$$

are the arguments which are used to detect the entropy violating cells in the y direction.

The values of ϕ, ϕ_x, ϕ_y at Gauss–Lobatto points and cell interface in (2.17) will be reconstructed by the fifth order HWENO method, which will be described in subsection 2.4. Then, we can rewrite the schemes (2.17) as $U_t = \mathcal{L}(U)$, where the $\mathcal{L}$ denotes the operator of spatial discretization, and use the third-order total variation diminishing (TVD) Runge–Kutta time discretization (2.4) to solve the semi-discrete form (2.17).

2.4. HWENO reconstruction in two dimensional case

In this subsection, we will describe the reconstruction procedures for ϕ, ϕ_x and ϕ_y at Gauss–Lobatto points and cell interface in (2.17) by HWENO method. We can use dimension-by-dimension strategy to reconstruct these point values. Now, we list the procedures of these reconstructions in the following.

Step 4. Reconstruction of $\{\phi\}$ at Gauss–Lobatto quadrature points in the cell $I_{i,j}$ by HWENO method from the cell averages $\{U_{i,j}, V_{i,j}, W_{i,j}, T_{i,j}\}$. We make the construction at the point $(x^-_{i+\frac{1}{2}}, y^-_{j+\frac{1}{2}})$ as example.

- We perform HWENO method which was described in Step 1 in subsection 2.2 in the x direction, from the cell average $\{U_{i,j}, V_{i,j}\}$, we can get $\frac{1}{\Delta y}\int_{K_j}\phi(x^-_{i+\frac{1}{2}}, y, t)dy$, which is the point value in x direction and the cell average in y direction.
- Then, we perform the similar procedure from the cell average $\{W_{i,j}, T_{i,j}\}$, we can get the one dimensional cell average $\frac{1}{\Delta y}\int_{K_j}\phi(x^-_{i+\frac{1}{2}}, y, t)\frac{y-y_j}{\Delta y}dy$.
- Finally, we perform the same HWENO method in the y direction, from $\{\frac{1}{\Delta y}\int_{K_j}\phi(x^-_{i+\frac{1}{2}}, y, t)dy\}$, and $\{\frac{1}{\Delta y}\int_{K_j}\phi(x^-_{i+\frac{1}{2}}, y, t)\frac{y-y_j}{\Delta y}dy\}$, we can get the point value $\phi(x^-_{i+\frac{1}{2}}, y^-_{j+\frac{1}{2}})$.

Remark.

(i). The reconstruction of $\{\phi\}$ at other Gauss–Lobatto quadrature points is similar to the procedure above.
(ii). When using the dimension-by-dimension strategy, the HWENO reconstruction procedures for point values at xG_2, xG_3 (or yG_2, yG_3) is similar to those for xG_1, xG_4 (or yG_1, yG_4), but the linear weights will become negative. For stability, the technique to treat the reconstruction procedure with negative weights is needed, for this technique we refer to [17].

Step 5. Reconstruction of $\{\phi_x\}$ at Gauss–Lobatto quadrature points in the cell $I_{i,j}$ by HWENO method from the cell averages $\{U_{i,j}, V_{i,j}, W_{i,j}, T_{i,j}\}$. Also, we make the construction at the point $(x^-_{i+\frac{1}{2}}, y^-_{j+\frac{1}{2}})$ as example.

- We perform HWENO method in Step 1 in subsection 2.2 in the y direction from the cell average $\{U_{i,j}, W_{i,j}\}$, which we can get the one dimensional cell average $\frac{1}{\Delta x}\int_{J_i}\phi(x, y^-_{j+\frac{1}{2}}, t)dx$.
- Then, we perform the similar procedure from the cell average $\{V_{i,j}, T_{i,j}\}$, which we can get the one dimensional cell average $\frac{1}{\Delta x}\int_{J_i}\phi(x, y^-_{j+\frac{1}{2}}, t)\frac{x-x_i}{\Delta x}dx$.
- Finally, we perform HWENO method in Step 2 in subsection 2.2 in the x direction from $\{\frac{1}{\Delta x}\int_{J_i}\phi(x, y^-_{j+\frac{1}{2}}, t)dx$, $\frac{1}{\Delta x}\int_{J_i}\phi(x, y^-_{j+\frac{1}{2}}, t)\frac{x-x_i}{\Delta x}dx\}$, we can get the point value $\phi_x(x^-_{i+\frac{1}{2}}, y^-_{j+\frac{1}{2}})$.

Remark.

(i). The reconstruction of $\{\phi_x\}$ at other Gauss–Lobatto quadrature points is also similar to the procedure above.
(ii). The procedure to reconstruct $\{\phi_y\}$ at Gauss–Lobatto quadrature points in the cell $I_{i,j}$ by HWENO method from the cell averages $\{U_{i,j}, V_{i,j}, W_{i,j}, T_{i,j}\}$, is similar to that for $\{\phi_x\}$, we will not repeat here.

Similar to one dimensional case, if H is a neither convex nor concave Hamiltonian, we also need the extra monotone modification in every Runge–Kutta step, which can help our method converge to the entropy solution. First, we should design the discontinuity indicator. Here we use the indicator [21] defined as follows:

$$\varphi^x_{i,j} = \frac{\beta^x_{i,j}}{\beta^x_{i,j} + \gamma^x_{i,j}}$$

where

$$\alpha^{1,x}_{i,j} = |X_{i-1,j} - X_{i,j}|^2 + \varepsilon \qquad \xi^{1,x}_{i,j} = |X_{i-1,j} - X_{i+1,j}|^2 + \varepsilon$$
$$\alpha^{2,x}_{i,j} = |X_{i,j-1} - X_{i,j}|^2 + \varepsilon \qquad \xi^{2,x}_{i,j} = |X_{i,j-1} - X_{i,j+1}|^2 + \varepsilon$$
$$\beta^x_{i,j} = \frac{\xi^{1,x}_{i,j}}{\alpha^{1,x}_{i-1,j}} + \frac{\xi^{1,x}_{i,j}}{\alpha^{1,x}_{i+2,j}} + \frac{\xi^{2,x}_{i,j}}{\alpha^{2,x}_{i,j-1}} + \frac{\xi^{2,x}_{i,j}}{\alpha^{2,x}_{i,j+2}}$$
$$\gamma^x_{i,j} = M\left(\frac{|X_{\max} - X_{\min}|^2}{\alpha^{1,x}_{i,j}} + \frac{|X_{\max} - X_{\min}|^2}{\alpha^{1,x}_{i+1,j}} + \frac{|X_{\max} - X_{\min}|^2}{\alpha^{2,x}_{i,j}} + \frac{|X_{\max} - X_{\min}|^2}{\alpha^{2,x}_{i,j+1}}\right)$$

and

$$\varphi_{i,j}^{y}=\frac{\beta_{i,j}^{y}}{\beta_{i,j}^{y}+\gamma_{i,j}^{y}}$$

where

$$\alpha_{i,j}^{1,y}=|Y_{i-1,j}-Y_{i,j}|^2+\varepsilon \qquad \xi_{i,j}^{1,y}=|Y_{i-1,j}-Y_{i+1,j}|^2+\varepsilon$$
$$\alpha_{i,j}^{2,y}=|Y_{i,j-1}-Y_{i,j}|^2+\varepsilon \qquad \xi_{i,j}^{2,y}=|Y_{i,j-1}-Y_{i,j+1}|^2+\varepsilon$$
$$\beta_{i,j}^{y}=\frac{\xi_{i,j}^{1,y}}{\alpha_{i-1,j}^{1,y}}+\frac{\xi_{i,j}^{1,y}}{\alpha_{i+2,j}^{1,y}}+\frac{\xi_{i,j}^{2,y}}{\alpha_{i,j-1}^{2,y}}+\frac{\xi_{i,j}^{2,y}}{\alpha_{i,j+2}^{2,y}}$$
$$\gamma_{i,j}^{y}=M\left(\frac{|Y_{\max}-Y_{\min}|^2}{\alpha_{i,j}^{1,y}}+\frac{|Y_{\max}-Y_{\min}|^2}{\alpha_{i+1,j}^{1,y}}+\frac{|Y_{\max}-Y_{\min}|^2}{\alpha_{i,j}^{2,y}}+\frac{|Y_{\max}-Y_{\min}|^2}{\alpha_{i,j+1}^{2,y}}\right)$$

and take $\phi_{i,j}=\max\{\varphi_{i,j}^{x},\varphi_{i,j}^{y}\}$, where, $X_{i,j}$ and $Y_{i,j}$ denote the cell average of ϕ_x of ϕ_y on $I_{i,j}$, respectively, which are computed by Gauss–Lobatto quadrature formula numerically, and $\varepsilon=10^{-6}$ in order to make sure the denominator would not be zero, and $X_{\max}$, $X_{\min}$, $Y_{\max}$ and $Y_{\min}$ are the maximum and minimum of $X_{i,j}$ and $Y_{i,j}$ respectively. M is a discontinuity parameter and we also choose $M=10000$. The discontinuity indicator $\varphi_{i,j}$ has the property that: (a). $0\le\varphi_{i,j}\le 1$; (b). $\varphi_{i,j}$ is $O(\Delta x^2,\Delta y^2)$ in smooth region; (c). $\varphi_{i,j}$ close to $O(1)$ near the derivative discontinuity. Now we modify our method as follows:

(1) Identify the neither convex nor concave troubled cell: we call cell I_{ij} a good cell if $\phi(x^{-}_{i+\frac{1}{2}},y^{-}_{j+\frac{1}{2}})$, $\phi(x^{+}_{i-\frac{1}{2}},y^{-}_{j+\frac{1}{2}})$, $\phi(x^{-}_{i+\frac{1}{2}},y^{+}_{j-\frac{1}{2}})$, $\phi(x^{+}_{i-\frac{1}{2}},y^{+}_{j-\frac{1}{2}})$ all fall into the same convex or concave region of the Hamiltonian $H(u,v)$, otherwise we define the cell as a troubled cell, see [16].

(2) If the cell I_{ij} is identified as a troubled cell, then $U_{i,j}^{n+1}$, $V_{i,j}^{n+1}$, $W_{i,j}^{n+1}$, $T_{i,j}^{n+1}$ should be modified. Introduce one order monotone scheme, again, we simply use the one order monotone scheme with Lax–Friedrichs Hamiltonian flux:

$$\begin{aligned}U_{i,j}^{n+1_{mono}}=U_{i,j}^{n}&-\Delta t\left(H\left(\frac{U_{i+1,j}^{n}-U_{i-1,j}^{n}}{2\Delta x},\frac{U_{i,j+1}^{n}-U_{i,j-1}^{n}}{2\Delta y}\right)\right)\\&+\frac{1}{2}\Delta t\alpha\left(\frac{U_{i+1,j}^{n}-2U_{i,j}^{n}+U_{i-1,j}^{n}}{\Delta x}\right)\\&+\frac{1}{2}\Delta t\beta\left(\frac{U_{i,j+1}^{n}-2U_{i,j}^{n}+U_{i,j-1}^{n}}{\Delta y}\right),\end{aligned}\tag{2.18}$$

where $\alpha=\max_u|H'_u(u,v)|$ and $\beta=\max_v|H'_v(u,v)|$.

(3) Modify $U_{i,j}^{n+1}$ with the monotone scheme. We combine the solution of (2.17) with (2.18) at $t=t^{n+1}$ convexly

$$U_{i,j}^{n+1_{mod}}=(1-\varphi_{i,j}^{2})U_{i,j}^{n+1}+\varphi_{i,j}^{2}U_{i,j}^{n+1_{mono}}.\tag{2.19}$$

For the same reason as the one dimensional case, the modification doesn't affect the fifth order accurate of the schemes. After modified procedure, we denote $U_{i,j}^{n+1_{mod}}$ as $U_{i,j}^{n+1}$.

(4) Modify $V_{i,j}^{n+1}$, $W_{i,j}^{n+1}$, $T_{i,j}^{n+1}$ by the following steps.

Step 6. Reconstruction of $V_{i,j}^{n+1_{mod}}$, $W_{i,j}^{n+1_{mod}}$, $T_{i,j}^{n+1_{mod}}$ by HWENO method from the cell averages $\{U_{i,j}^{n+1},V_{i,j}^{n+1},W_{i,j}^{n+1},T_{i,j}^{n+1}\}$

The reconstructions of $V_{i,j}^{n+1_{mod}}$ and $W_{i,j}^{n+1_{mod}}$ were performed in x direction and y direction by one dimensional fifth order HWENO method which is described in Step 3 in subsection 2.2 from cell average $\{U_{i,j}^{n+1},V_{i,j}^{n+1}\}$ and $\{U_{i,j}^{n+1},W_{i,j}^{n+1}\}$, respectively. Again we denote $V_{i,j}^{n+1_{mod}}$ and $W_{i,j}^{n+1_{mod}}$ as $V_{i,j}^{n+1}$ and $W_{i,j}^{n+1}$.

The procedure to reconstruct $T_{i,j}^{n+1_{mod}}$ is divided into two parts; firstly we perform the reconstruction Step 3 in x direction from $\{U_{i,j}^{n+1},V_{i,j}^{n+1}\}$, $\{W_{i,j}^{n+1},T_{i,j}^{n+1}\}$, and obtain the new cell average $\widetilde{V}_{i,j}^{n+1}$, $\widetilde{T}_{i,j}^{n+1}$, then we perform the reconstruction Step 3 in y direction from $\{\widetilde{V}_{i,j}^{n+1},\widetilde{T}_{i,j}^{n+1}\}$ and obtain $T_{i,j}^{n+1_{mod}}$, which is also denoted as $T_{i,j}^{n+1}$.

Table 1
$\phi_t + \phi_x = 0, \phi(x,0) = \sin(\pi x)$. Periodic boundary conditions. $t = 2$.

N	L_∞ error	L_∞ order	L_1 error	L_1 order
10	1.92E−03		8.47E−04	
20	6.01E−05	5.00	2.66E−05	4.99
40	1.89E−06	4.99	8.22E−07	5.02
80	5.79E−08	5.03	2.57E−08	5.00
160	1.63E−09	5.15	8.04E−10	5.00
320	4.08E−11	5.32	2.52E−11	5.00

Table 2
$\phi_t + \sin(x)\phi_x = 0, \phi(x,0) = \sin(x)$. Periodic boundary conditions. $t = 1$.

N	L_∞ error	L_∞ order	L_1 error	L_1 order
10	5.76E−02		1.24E−02	
20	4.85E−04	6.89	1.12E−04	6.79
40	5.91E−05	3.04	5.09E−06	4.46
80	1.22E−06	5.59	1.32E−07	5.27
160	2.38E−08	5.69	3.49E−09	5.24
320	4.00E−10	5.89	9.17E−11	5.25

3. Numerical result

In this section, we provide the numerical experiments for fifth order HWENO method in one dimension and two dimension. In all numerical experiments, we set $\Delta t = 0.8\Delta x^{\frac{5}{3}}$ in the one dimensional case and $\Delta t = 0.8\frac{1}{\frac{\alpha}{(\Delta x)^{5/3}} + \frac{\beta}{(\Delta y)^{5/3}}}$ in the two dimensional case, where $\alpha = \max_u |H'_u(u,v)|$ and $\beta = \max_v |H'_v(u,v)|$, in order to guarantee that spatial numerical errors are dominated.

3.1. One dimensional case with accurate test

Example 3.1. We solve the following linear scalar equation:

$$\phi_t + \phi_x = 0, \qquad 0 \le x \le 2$$

with the initial condition $\phi(x,0) = \sin(\pi x)$, and periodic boundary condition. We compute the solution up to $t = 2$, the numerical errors and numerical order of HWENO method are shown in Table 1. We can see that the scheme achieves our design accuracy.

Example 3.2. We solve the following variable coefficient linear equation:

$$\phi_t + \sin(x)\phi_x = 0, \qquad 0 < x < 2\pi$$

with the initial condition $\phi(x,0) = \sin(x)$, and periodic boundary condition, see [22]. The exact solution is

$$\phi(x,t) = \sin(2\arctan(e^{-t}\tan(\frac{x}{2})))$$

We compute the solution up to $t = 1$, the numerical errors and numerical order of HWENO method are shown in Table 2. Again, we observe that, the fifth order is obtained by HWENO method.

Example 3.3. We solve the Burgers equation:

$$\phi_t + \frac{1}{2}(\phi_x + 1)^2 = 0, \qquad -1 \le x \le 1$$

with the initial condition $\phi(x,0) = -\cos(\pi x)$, and periodic boundary condition. We compute the solution up to $t = \frac{0.5}{\pi^2}$. At this time, the solution is still smooth. The numerical results are shown in Table 3. Again, we can see the scheme meet our design accuracy.

Example 3.4. We solve the nonlinear scalar equation:

$$\phi_t - \cos(\phi_x + 1) = 0, \qquad -1 < x < 1$$

with the initial condition $\phi(x,0) = -\cos(\pi x)$, and periodic boundary condition. When $t = \frac{0.5}{\pi^2}$, the solution is still smooth. The numerical results are shown in Table 4. As the Hamiltonian $H(u) = -\cos(u+1)$ is neither convex nor concave, the monotone modification is used. Again, we observe that the scheme can achieve its design accuracy both with and without the monotone modification.

Table 3
$\phi_t + \frac{1}{2}(\phi_x + 1)^2 = 0, \phi(x,0) = -\cos(\pi x)$. Periodic boundary conditions. $t = 0.5/\pi^2$.

N	L_∞ error	L_∞ order	L_1 error	L_1 order
10	3.64E−03		5.62E−04	
20	2.97E−04	3.61	2.27E−05	4.63
40	3.04E−06	6.61	2.98E−07	6.25
80	5.38E−08	5.82	4.38E−09	6.09
160	8.22E−10	6.03	7.58E−11	5.85
320	8.54E−12	6.59	1.88E−12	5.34

Table 4
$\phi_t - \cos(\phi_x + 1) = 0, \phi(x,0) = -\cos(\pi x)$. Periodic boundary conditions. $t = 0.5/\pi^2$.

N	With the monotone modification				Without the monotone modification			
	L_∞ error	L_∞ order	L_1 error	L_1 order	L_∞ error	L_∞ order	L_1 error	L_1 order
10	6.71E−03		2.96E−03		7.48E−03		1.08E−03	
20	3.65E−04	4.20	9.77E−05	4.92	2.34E−04	5.00	3.05E−05	5.15
40	3.00E−05	3.60	2.71E−06	5.17	3.14E−05	2.90	1.40E−06	4.45
80	1.21E−06	4.63	8.67E−08	4.97	1.06E−06	4.88	3.09E−08	5.50
160	9.58E−08	3.66	2.69E−09	5.01	1.61E−08	6.05	5.13E−10	5.91
320	2.84E−09	5.07	5.52E−11	5.61	2.22E−10	6.18	8.50E−12	5.91

3.2. One dimensional case with discontinuous derivative

Example 3.5. We solve the linear equation:

$$\phi_t + \phi_x = 0$$

with the initial condition $\phi(x,0) = \phi_0(x - 0.5)$ together with the periodic boundary condition, where

$$\phi_0(x) = -(\frac{\sqrt{3}}{2} + \frac{9}{2} + \frac{2\pi}{3})(x+1) + \begin{cases} 2\cos(\frac{3\pi x^2}{2}) - \sqrt{3} & -1 \le x < -\frac{1}{3}, \\ \frac{3}{2} + 3\cos(2\pi x) & -\frac{1}{3} \le x < 0, \\ \frac{15}{2} - 3\cos(2\pi x) & 0 \le x < \frac{1}{3}, \\ \frac{28 + 4\pi + \cos(3\pi x)}{3} + 6\pi x(x-1) & \frac{1}{3} \le x < 1. \end{cases}$$

We plot the result at $t = 2.0$ and $t = 8.0$ in Fig. 1(a) and Fig. 1(b) respectively. We observe that the HWENO schemes have good resolution for the corner singularity.

Example 3.6. We solve the problem:

$$\phi_t + \text{sign}(\cos(x))\phi_x = 0 \qquad 0 \le x \le 2\pi$$

with initial $\phi(x,0) = \sin(x)$ and periodic boundary condition [2]. For the viscosity solution, a shock and a rarefaction wave are forming at $x = \pi/2$ and $x = 3\pi/2$, respectively. We compute the errors in smooth region $[0,1] \bigcup [2, 3.4] \bigcup [6, 2\pi]$, and the result is listed in Table 5. We can see that the method reach the fifth order accurate as we expect. We also plot the result at time $t = 1.0$ with mesh $N = 40$ and $N = 80$ in Fig. 2(a) and Fig. 2(b) respectively. We observe that the HWENO schemes can converge to the viscosity solution.

Example 3.7. We solve one dimensional Burgers' equation:

$$\phi_t + \frac{1}{2}(\phi_x + 1)^2 = 0 \qquad -1 \le x \le 1$$

with $\phi(x,0) = -\cos(\pi x)$ and periodic boundary conditions. We compute the solution up to $t = 3.5/\pi^2$. At this time, the discontinuous derivative has already appeared in the solution. We compute the L_1 and L_∞ in smooth region $[-1, -0.95] \bigcup [-0.35, 1]$, the result is listed in Table 6. We can see that the method reach the fifth order accurate as we expect. Also, we show the numerical results with mesh $N = 40$ and $N = 80$ in Fig. 3(a) and Fig. 3(b) respectively. We can see that the schemes give good results for this problem.

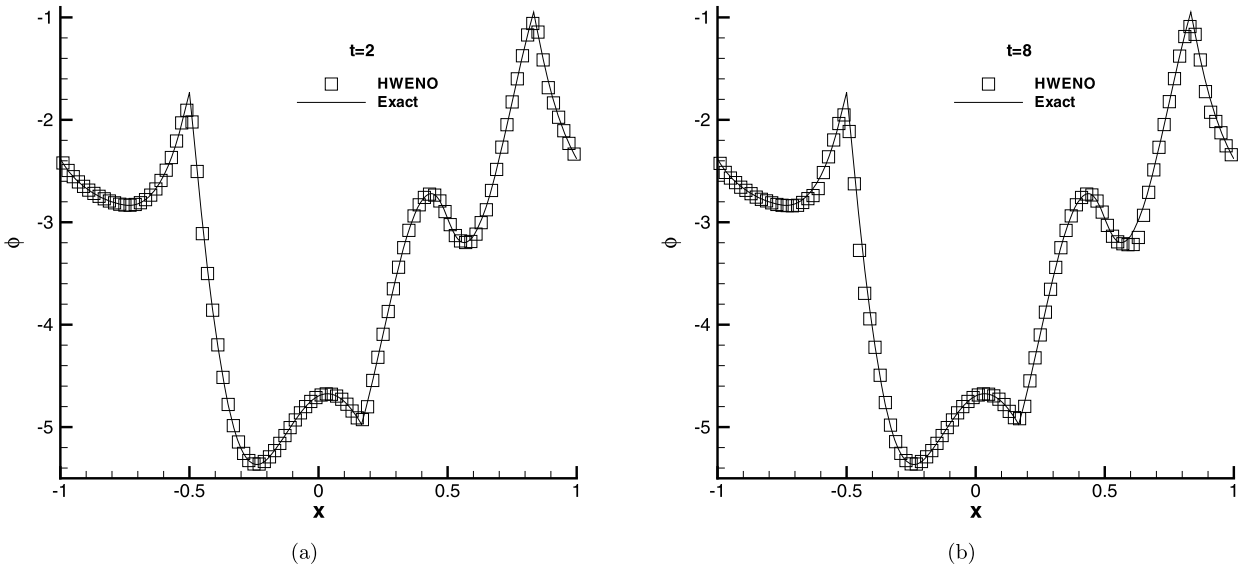

Fig. 1. One dimensional linear equation. $N = 100$ cells. (a). $t = 2.0$, (b). $t = 8.0$. Solid line: the exact solution; Square symbol: the HWENO scheme.

Table 5
$\phi_t + \text{sign}(\cos(x))\phi_x = 0, \phi(x, 0) = \sin(x)$. Periodic boundary conditions. $t = 1$.

N	L_∞ error	L_∞ order	L_1 error	L_1 order
10	3.66E−03		2.69E−03	
20	3.51E−04	3.99	1.68E−04	4.72
40	8.44E−05	2.06	1.79E−05	3.23
80	4.92E−06	4.28	5.75E−07	5.17
160	2.45E−07	4.33	6.64E−09	6.43
320	5.84E−10	8.90	3.65E−11	7.67

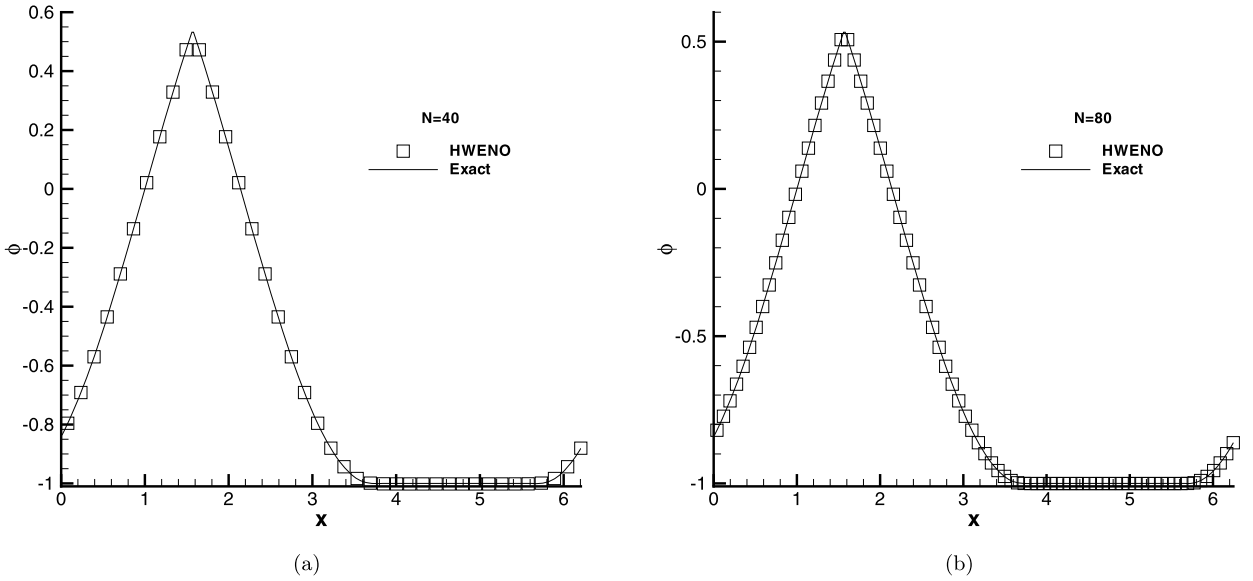

Fig. 2. One dimensional linear problem with non-smooth variable coefficient. $t = 1$. (a). $N = 40$ and (b). $N = 80$. Solid line: the exact solution; Square symbol: the HWENO scheme.

Example 3.8. We solve nonlinear equation with a non-convex flux

$$\phi_t - \cos(\phi_x + 1) = 0$$

with the initial data $\phi(x, 0) = -\cos(\pi x)$ and periodic boundary conditions. This time, we compute the solution up to $t = 1.5/\pi^2$. As the Hamiltonian $H(u) = -\cos(u + 1)$ is neither convex nor concave, we use the monotone modification in

Table 6
$\phi_t + \frac{1}{2}(\phi_x + 1)^2 = 0, \phi(x, 0) = -\cos(\pi x)$. Periodic boundary conditions. $t = 3.5/\pi^2$.

N	L_∞ error	L_∞ order	L_1 error	L_1 order
10	2.19E−04		9.38E−05	
20	6.18E−06	5.68	1.35E−06	6.74
40	1.58E−07	5.29	2.74E−08	5.63
80	1.43E−09	7.14	6.61E−10	5.65
160	4.37E−11	5.16	1.97E−11	5.19
320	1.36E−12	5.07	6.12E−13	5.08

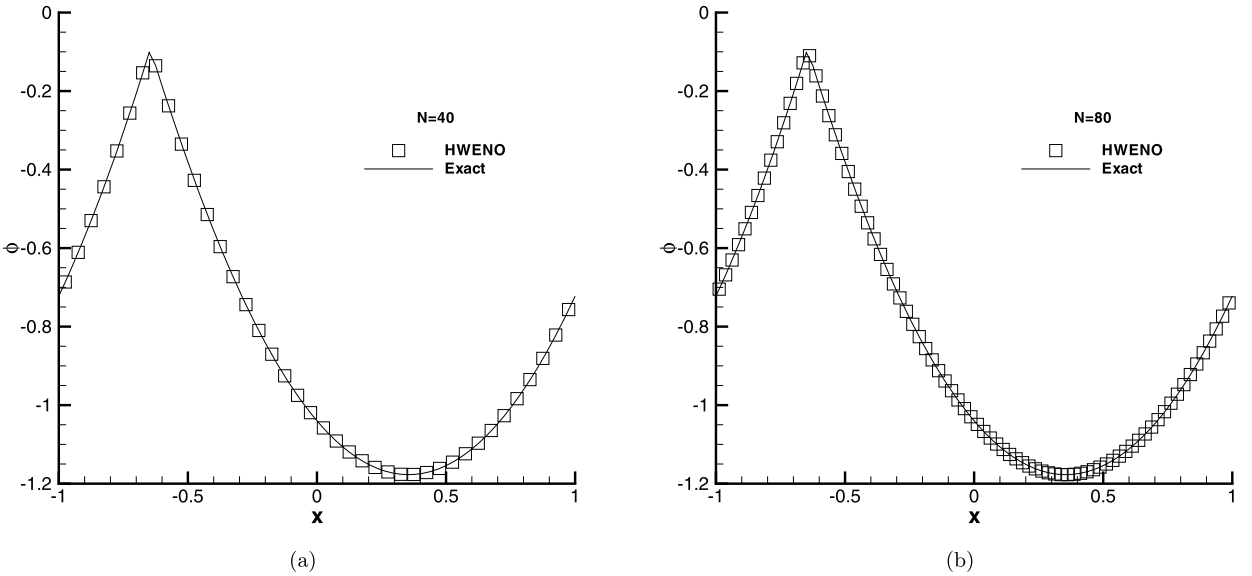

Fig. 3. One dimensional Burgers' equation. $t = 3.5/\pi^2$. (a). $N = 40$ and (b). $N = 80$. Solid line: the exact solution; Square symbol: the HWENO scheme.

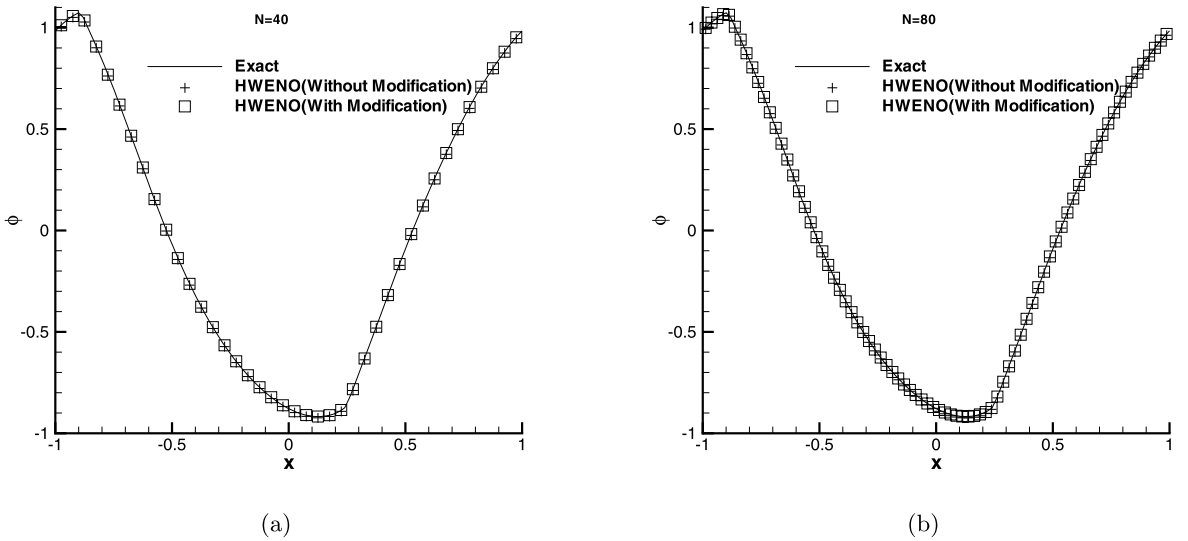

Fig. 4. $H(u) = -\cos(u + 1)$. $t = 1.5/\pi^2$. (a). $N = 40$ and (b). $N = 80$. Solid line: the exact solution; Square symbol: the HWENO scheme with modification; Plus symbol: the HWENO scheme without modification.

this case. However, we observe the figures before and after the monotone modification with $N = 40$ and $N = 80$, which are shown in Fig. 4, and find that the modification is dispensable in this case. In fact, only Examples 3.9 and 3.16 in this paper absolutely need the monotone modification. We also record the troubled cell rate at each time level, which is shown in Fig. 5, the average of the troubled cells rate at all time levels is 10.62% for $N = 40$ and 5.174% for $N = 80$ respectively.

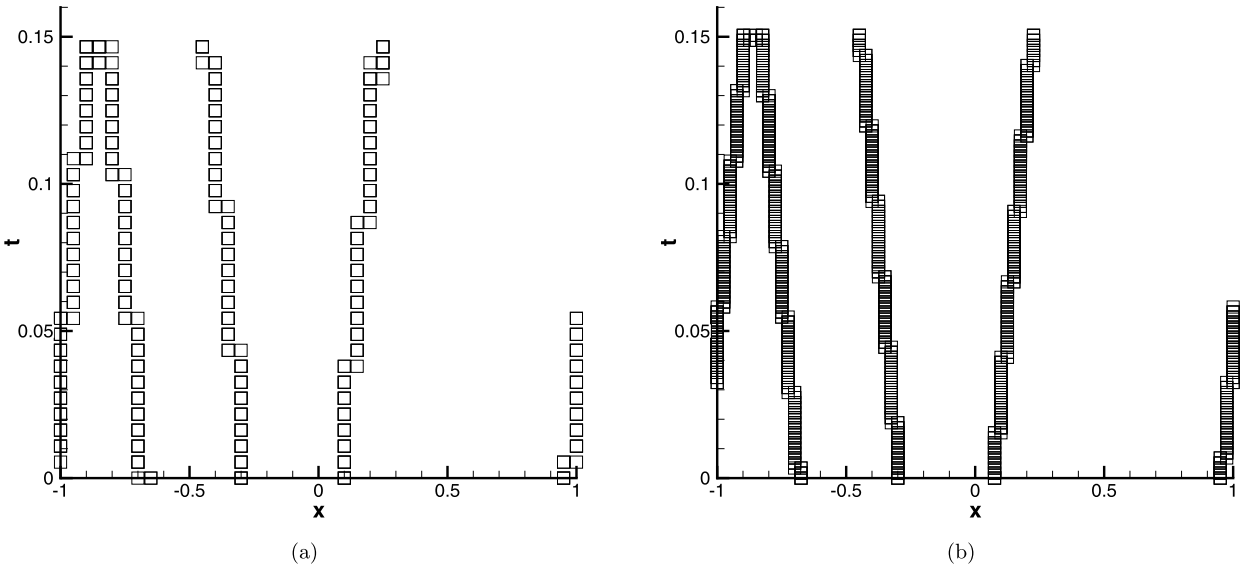

Fig. 5. The troubled cell at each time level when $N = 40$ and $N = 80$. Square symbol: the troubled cell.

Table 7
$\phi_t - \cos(\phi_x + 1) = 0, \phi(x, 0) = -\cos(\pi x)$. Periodic boundary conditions. $t = 1.5/\pi^2$.

N	With the monotone modification				Without the monotone modification			
	L_∞ error	L_∞ order	L_1 error	L_1 order	L_∞ error	L_∞ order	L_1 error	L_1 order
10	2.02E−02		5.67E−03		9.54E−03		4.34E−03	
20	1.36E−03	4.68	3.82E−04	4.69	1.41E−03	3.32	4.73E−04	3.86
40	4.10E−04	2.02	4.12E−05	3.74	3.20E−04	2.49	3.86E−05	4.21
80	2.63E−05	4.29	1.75E−06	4.93	2.57E−05	3.94	1.75E−06	4.83
160	7.29E−07	5.39	4.35E−08	5.56	7.29E−07	5.36	4.35E−08	5.55
320	1.06E−08	6.23	1.02E−09	5.52	1.06E−08	6.23	1.02E−09	5.52

Table 8
$\phi_t + \frac{1}{4}(\phi_x^2 - 1)(\phi_x^2 - 4) = 0, \phi(x, 0) = -2|x|$. $t = 1$.

N	Even				N	Odd			
	L_∞ error	Order	L_1 error	Order		L_∞ error	Order	L_1 error	Order
10	2.80E−01		9.43E−02		11	5.73E−02		1.74E−02	
20	9.17E−02	1.90	1.10E−02	3.66	21	2.88E−02	1.17	3.30E−03	2.82
40	4.39E−03	4.78	2.60E−04	5.89	41	8.64E−04	5.51	6.04E−05	6.29
80	4.53E−05	6.90	1.46E−06	7.81	81	1.19E−05	5.93	4.71E−07	6.72
160	1.44E−07	8.12	2.71E−09	8.88	161	5.67E−08	8.23	1.77E−09	8.60
320	1.90E−09	6.17	3.06E−11	6.40	321	8.86E−10	5.94	4.66E−11	5.19

Finally, we compute the error in smooth region $[-0.7, 0.0] \bigcup [0.4, 1]$, the result is listed in Table 7. We can see that the method reach the expected precision.

Example 3.9. We solve the problem

$$\phi_t + \frac{1}{4}(\phi_x^2 - 1)(\phi_x^2 - 4) = 0 \qquad -1 < x < 1$$

with initial data $\phi(x, 0) = -2|x|$. The Hamiltonian $H(u) = \frac{1}{4}(u^2 - 1)(u^2 - 4)$ is neither convex nor concave, and the monotone modification is indispensable in this case. We compute error in smooth area $[-1, -0.58] \bigcup [0.58, 1]$ for odd and even values of N, which is shown in Table 8, and we observe that this method can reach fifth precision. Fig. 6 list the result with and without modification at $t = 1$ with $N = 80$ and $N = 81$ by our scheme. The different behaviors result from the singular point $x = 0$ is exactly located at the cell interface when N is even while the point is inside the cell when N is odd at $t = 0$. We observe that the method with monotone modification can correctly converge to the viscosity solution for both even and odd N. We also record the troubled cell rate at each time level, which is shown at Fig. 7, and the average of the troubled cells rate at all time levels is 3.120% and 3.090% for $N = 80$ and $N = 81$ respectively.

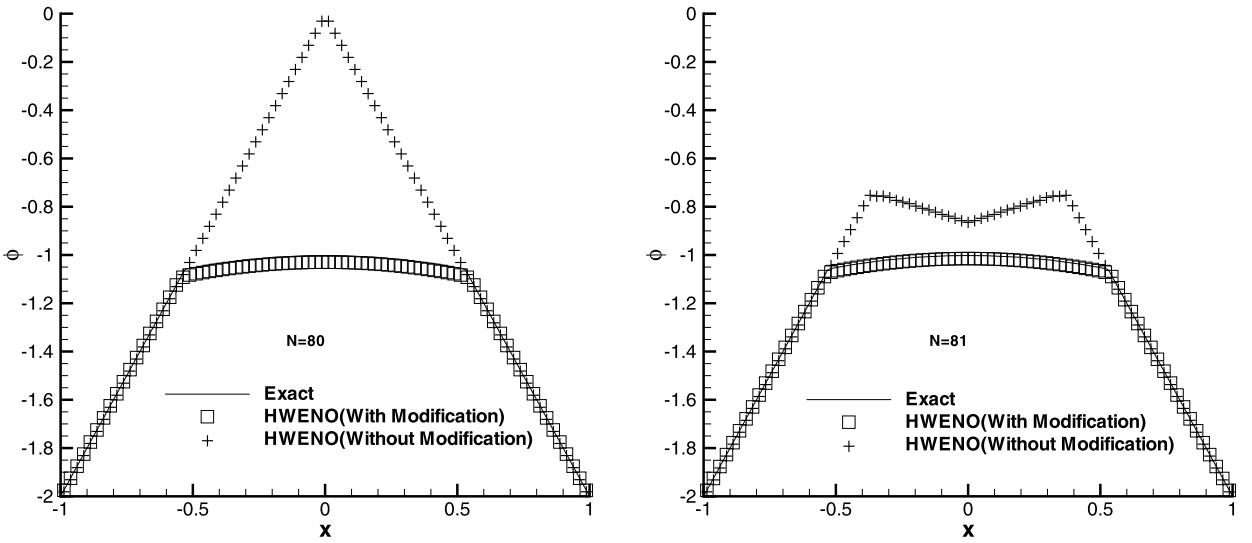

Fig. 6. $H(u) = (1/4)(u^2-1)(u^2-4)$. $t = 1$. (a). $N = 80$ and (b). $N = 81$. Solid line: the exact solution; Square symbol: the HWENO scheme with modification; Plus symbol: the HWENO scheme without modification.

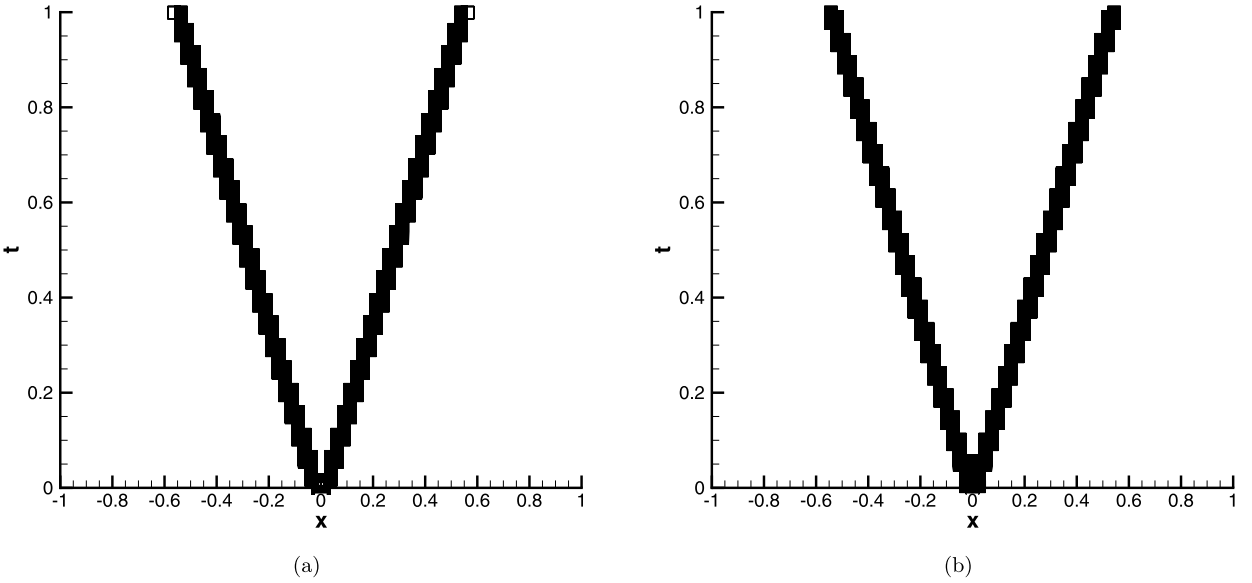

Fig. 7. The troubled cell at each time level when $N = 80$ and $N = 81$. Square symbol: the troubled cell.

3.3. Two dimensional case with accurate test

Example 3.10. We solve the two dimensional linear scaler equation.

$$\phi_t + \phi_x + \phi_y = 0 \qquad -2 \le x, y \le 2$$

with initial data $\phi(x, y, 0) = \sin(\pi(x+y)/2)$ and periodic condition. The result when $t = 2$ is listed in Table 9. We see that the schemes can achieve the design accuracy.

Example 3.11. We solve the two dimensional Burgers' equation

$$\phi_t + \frac{1}{2}(\phi_x + \phi_y + 1)^2 = 0 \qquad -2 \le x, y \le 2$$

with initial data $\phi(x, y, 0) = -\cos(\frac{\pi}{2}(x+y))$ and periodic condition. We compute the result up to $t = 0.5/\pi^2$ and the solution is still smooth at that time. Again, from Table 10, we can see the scheme can achieve the design order.

Table 9
$\phi_t + \phi_x + \phi_y = 0, \phi(x, y, 0) = \sin(\pi(x + y)/2)$. Periodic boundary conditions. $t = 2$.

N	L_∞ error	L_∞ order	L_1 error	L_1 order
10×10	5.82E−03		3.44E−03	
20×20	1.83E−04	4.99	1.07E−04	5.01
40×40	5.82E−06	4.98	3.32E−06	5.01
80×80	1.82E−07	5.00	1.04E−07	5.00
160×160	5.48E−09	5.05	3.23E−09	5.00
320×320	1.60E−10	5.09	1.01E−10	5.00

Table 10
$\phi_t + \frac{1}{2}(\phi_x + \phi_y + 1)^2 = 0$, $\phi(x, y, 0) = -\cos(\frac{\pi}{2}(x + y))$. Periodic boundary conditions. $t = 0.5/\pi^2$.

N	L_∞ error	L_∞ order	L_1 error	L_1 order
10×10	3.36E−03		9.14E−04	
20×20	3.87E−04	3.12	3.21E−05	4.83
40×40	6.37E−06	5.92	6.47E−07	5.63
80×80	1.20E−07	5.73	1.21E−08	5.74
160×160	1.82E−09	6.05	2.55E−10	5.56
320×320	3.30E−11	5.78	6.86E−12	5.22

Table 11
$\phi_t - \cos(\phi_x + \phi_y + 1) = 0$, $\phi(x, y, 0) = -\cos(\frac{\pi}{2}(x + y))$. Periodic boundary conditions. $t = 0.5/\pi^2$.

N	With monotone modify				Without monotone modify			
	L_∞ error	L_∞ order	L_1 error	L_1 order	L_∞ error	L_∞ order	L_1 error	L_1 order
10×10	4.10E−02		8.73E−03		1.53E−02		2.31E−03	
20×20	8.11E−04	5.66	1.37E−04	5.99	5.69E−04	4.75	5.96E−05	5.28
40×40	6.65E−05	3.61	6.50E−06	4.40	6.15E−05	3.21	2.87E−06	4.38
80×80	5.36E−06	3.63	1.82E−07	5.16	2.04E−06	4.91	6.37E−08	5.49
160×160	1.98E−07	4.76	3.90E−09	5.55	3.53E−08	5.85	1.17E−09	5.76
320×320	6.00E−09	5.05	7.21E−11	5.76	4.99E−10	6.15	2.17E−11	5.75

Table 12
$\phi_t + \frac{1}{2}(\phi_x + \phi_y + 1)^2 = 0$, $\phi(x, y, 0) = -\cos(\frac{\pi}{2}(x + y))$. Periodic boundary conditions. $t = 1.5/\pi^2$.

N	L_∞ error	L_∞ order	L_1 error	L_1 order
10×10	1.93E−04		1.02E−04	
20×20	2.18E−05	3.15	3.64E−06	4.81
40×40	1.06E−06	4.36	1.34E−07	4.77
80×80	4.57E−08	4.53	4.62E−09	4.86
160×160	1.66E−09	4.78	1.54E−10	4.90
320×320	5.62E−11	4.88	6.63E−12	4.54

Example 3.12.

$$\phi_t - \cos(\phi_x + \phi_y + 1) = 0 \qquad -2 \le x, y \le 2$$

with initial data $\phi(x, 0) = -\cos(\frac{\pi}{2}(x + y))$ with periodic condition. We also compute the result up to $t = 0.5/\pi^2$ and the solution is still smooth at that time. The Hamiltonian $H(u, v) = -\cos(u + v + 1)$ is neither convex nor concave, so we use the monotone modification. Again, from Table 11 we can see the scheme can achieve the design order both with and without the modification.

3.4. Two dimensional case with discontinuous derivative

Example 3.13. We solve the two dimensional Burgers' equation

$$\phi_t + \frac{1}{2}(\phi_x + \phi_y + 1)^2 = 0 \qquad -2 \le x, y \le 2$$

with initial data $\phi(x, y, 0) = -\cos(\frac{\pi}{2}(x + y))$. We compute the result up to $t = 1.5/\pi^2$ and the derivative discontinuity is appeared in the solution. Numerical error is shown in Table 12, which is computed in smooth subregion $[0, 1.2] \times [-0.4, 0.8]$, we observe that the result can achieve the fifth precision. We also plot the results with 40×40 cells in Fig. 8(a) and Fig. 8(b). We observe good resolutions in this example.

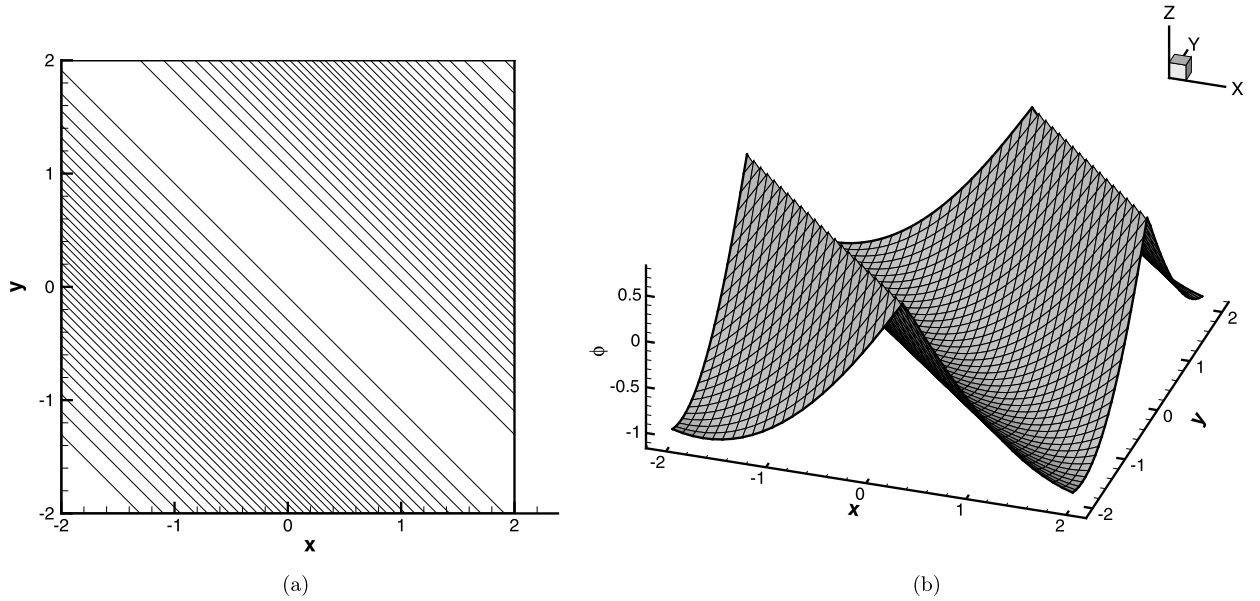

Fig. 8. Two dimensional Burgers equation. $t = 1.5/\pi^2$ with the HWENO schemes with 40×40 cells. Contours of the solution (a) and the surface of the solution (b).

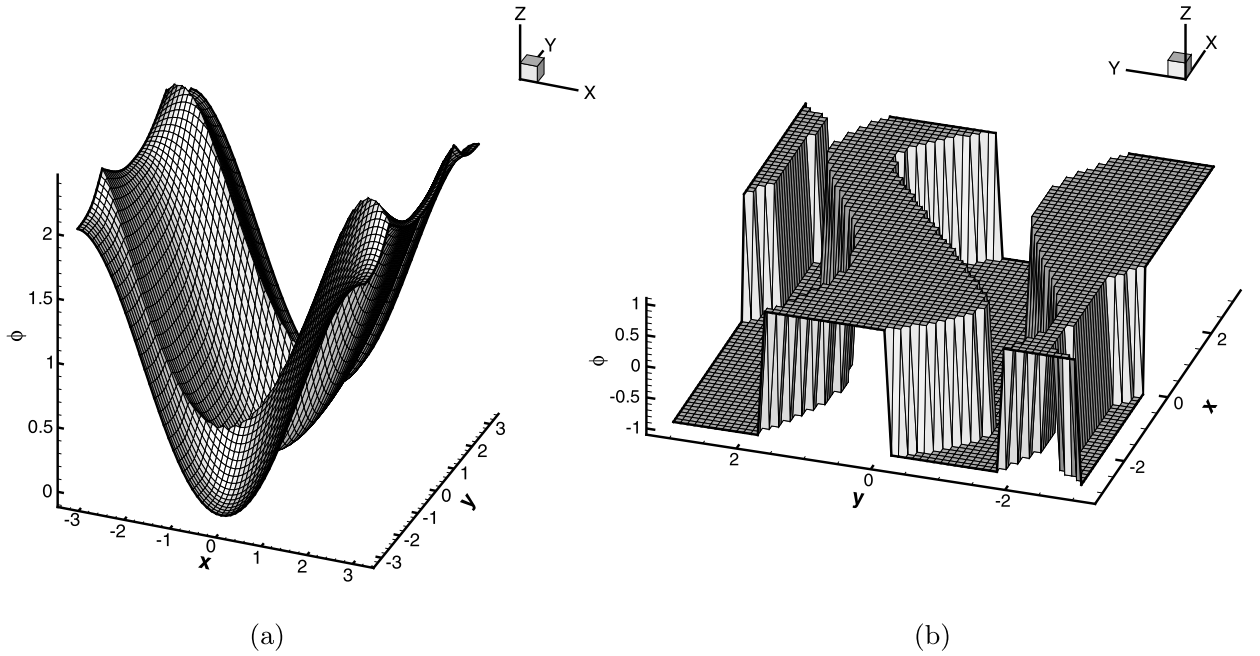

Fig. 9. The optimal control problem. $t = 1$ with the HWENO schemes with 60×60 cells. Surface of the solution (a) and of the optimal control $\omega = \text{sign}(\phi_y)$ (b).

Example 3.14. We solve the problem from optimal control:

$$\phi_t + \sin(y)\phi_x + (\sin(x) + \text{sign}(\phi_y))\phi_y - \frac{1}{2}\sin^2(y) + \cos(x) - 1 = 0, \quad -\pi < x, y < \pi$$

with $\phi(x, y, 0) = 0$ and periodic conditions. The solution is plotted at $t = 1$ and the optimal control $\omega = \text{sign}(\phi)$ are shown is Fig. 9(a) and Fig. 9(b), respectively. Again, we can observe the good resolution is achieved by our method.

Example 3.15. We solve the problem

$$\phi_t - \cos(\phi_x + \phi_y + 1) = 0, \qquad -2 < x, y < 2$$

Table 13
$\phi_t - \cos(\phi_x + \phi_y + 1) = 0$, $\phi(x, y, 0) = -\cos(\frac{\pi}{2}(x + y))$. Periodic boundary conditions. $t = 1.5/\pi^2$.

N	With monotone modify				Without monotone modify			
	L_∞ error	L_∞ order	L_1 error	L_1 order	L_∞ error	L_∞ order	L_1 error	L_1 order
10×10	4.10E−02		8.73E−03		1.53E−02		2.31E−03	
20×20	8.11E−04	5.66	1.37E−04	5.99	5.69E−04	4.75	5.96E−05	5.28
40×40	6.65E−05	3.61	6.50E−06	4.40	6.15E−05	3.21	2.87E−06	4.38
80×80	5.36E−06	3.63	1.82E−07	5.16	2.04E−06	4.91	6.37E−08	5.49
160×160	1.98E−07	4.76	3.90E−09	5.55	3.53E−08	5.85	1.17E−09	5.76
320×320	6.00E−09	5.05	7.21E−11	5.76	4.99E−10	6.15	2.17E−11	5.75

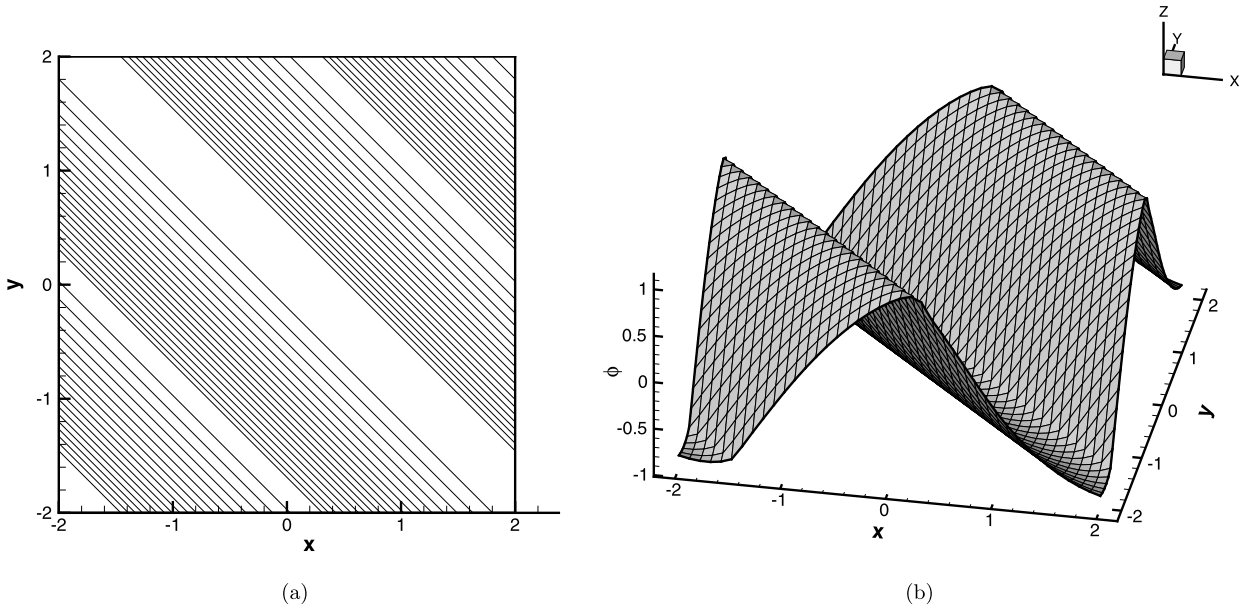

(a) (b)

Fig. 10. Two dimensional equation with a neither convex nor concave Hamiltonian. $t = 1.5/\pi^2$ with the HWENO schemes with 40×40 cells. Contours of the solution (a) and surface of the solution (b).

with $\phi(x, y, 0) = -\cos(\frac{\pi}{2}(x + y))$ and periodic conditions. We also compute the solution up to $t = 1.5/\pi^2$ and the solution develop the discontinuous derivative. Although the Hamiltonian is neither convex nor concave in this case, the modification is dispensable. We compute the numerical error in subregion $[0, 0.4] \times [-0.4, 0]$, which is shown in Table 13. Fifth precision is achieved by our method. The results with 40×40 cells by HWENO method after modification are shown in Fig. 10(a) and Fig. 10(b). We observe good resolutions for this example. We record the troubled cells rate at each time level, the average of the troubled cells rate at all time levels is 19.75%. See Fig. 11.

Example 3.16. We solve the problem with neither convex nor concave Hamiltonian

$$\phi_t + \sin(\phi_x + \phi_y) = 0, \qquad -1 < x, y < 1$$

with $\phi(x, y, 0) = \pi(|y| - |x|)$. The monotone modification is indispensable in this case. The solution are shown in Fig. 12. Again, we observe good resolution for this example. We record the troubled cells rate at each time level, the average of the troubled cells rate at all time levels is 45.45%. See Fig. 13.

Example 3.17. We solve the two dimensional Eikonal equation

$$\phi_t + \sqrt{\phi_x^2 + \phi_y^2 + 1} = 0, \qquad 0 \le x, y < 1$$

with the initial data $\phi(x, y, 0) = \frac{1}{4}(\cos(2\pi x) - 1)(\cos(2\pi y) - 1) - 1$. The solution are shown in Fig. 14(a) and 14(b) respectively. We observe good resolutions for this example.

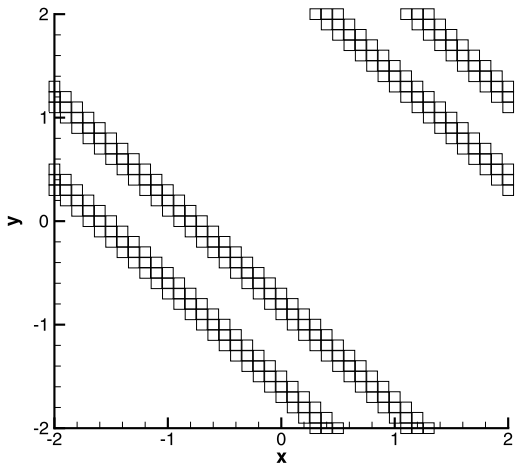

Fig. 11. The troubled cells at $t = 1.5/\pi^2$. Square symbol: the troubled cell.

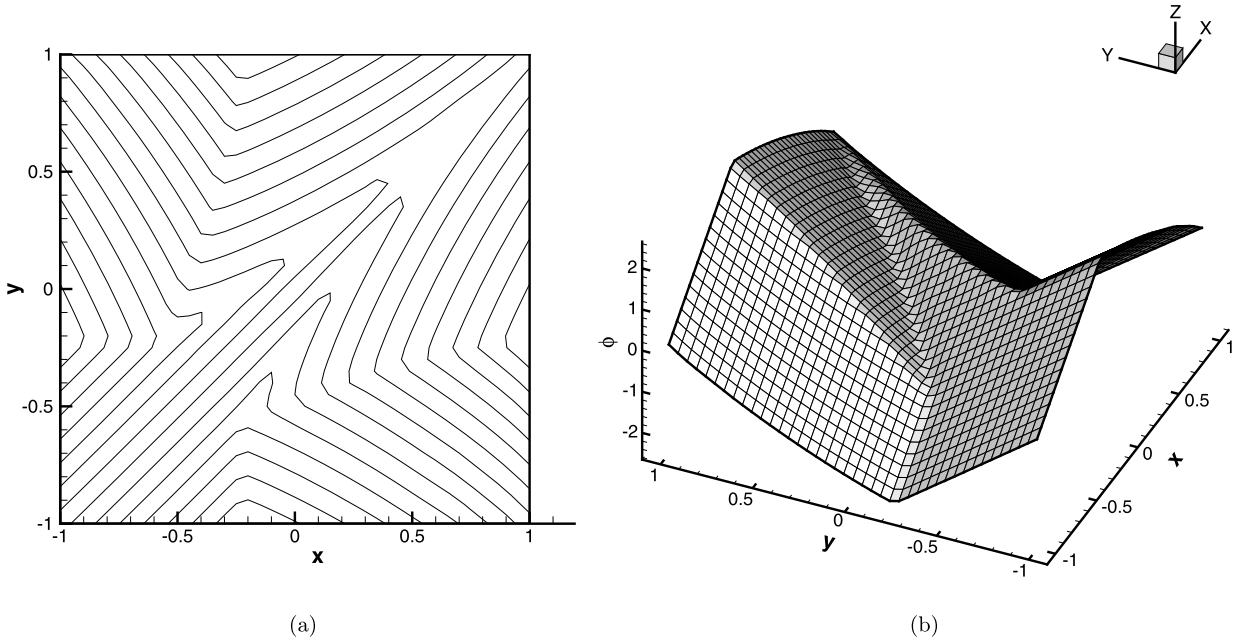

(a) (b)

Fig. 12. Two dimensional equation with a neither convex nor concave Hamiltonian. $t = 1$ by the HWENO schemes with 40×40 cells. Contours of the solution (a) and surface of the solution (b).

Example 3.18.

$$\begin{cases} \phi_t - (1 - \varepsilon K)\sqrt{\phi_x^2 + \phi_y^2 + 1} = 0, \quad 0 \le x, y < 1 \\ \phi(x, y, 0) = 1 - \dfrac{1}{4}(\cos(2\pi x) - 1)(\cos(2\pi y) - 1) \end{cases}$$

where K is the mean curvature defined by:

$$K = -\frac{\phi_{xx}(1 + \phi_y^2) - 2\phi_{xy}\phi_x\phi_y + \phi_{yy}(1 + \phi_x^2)}{(1 + \phi_x^2 + \phi_y^2)^{3/2}}$$

and ε is a small constant, the initial data $\phi(x, y, 0) = 1 - \frac{1}{4}(\cos(2\pi x) - 1)(\cos(2\pi y) - 1)$ and the periodic condition. The approximation of the second derivatives are constructed by the method similar to that of the first derivative terms. The results of $\varepsilon = 0$ (pure convection) and $\varepsilon = 0.1$ by the HWENO method with 60×60 cells are presented in Fig. 15(a) and Fig. 15(b). The surfaces at $t = 0$ for $\varepsilon = 0$ and for $\varepsilon = 0.1$, and at $t = 0.1$ for $\varepsilon = 0.1$, are shifted downward in order to show the detail of the solution at later time.

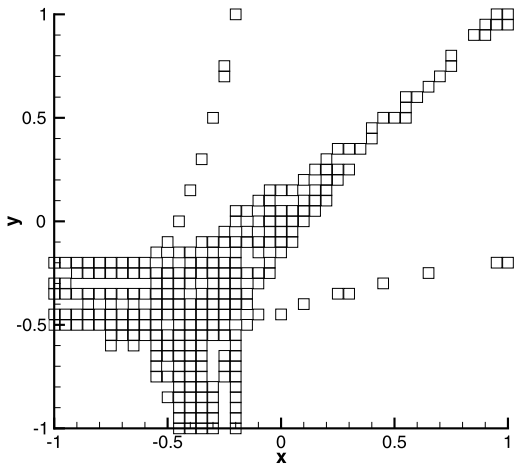

Fig. 13. The troubled cell at $t = 1$. Square symbol: the troubled cell.

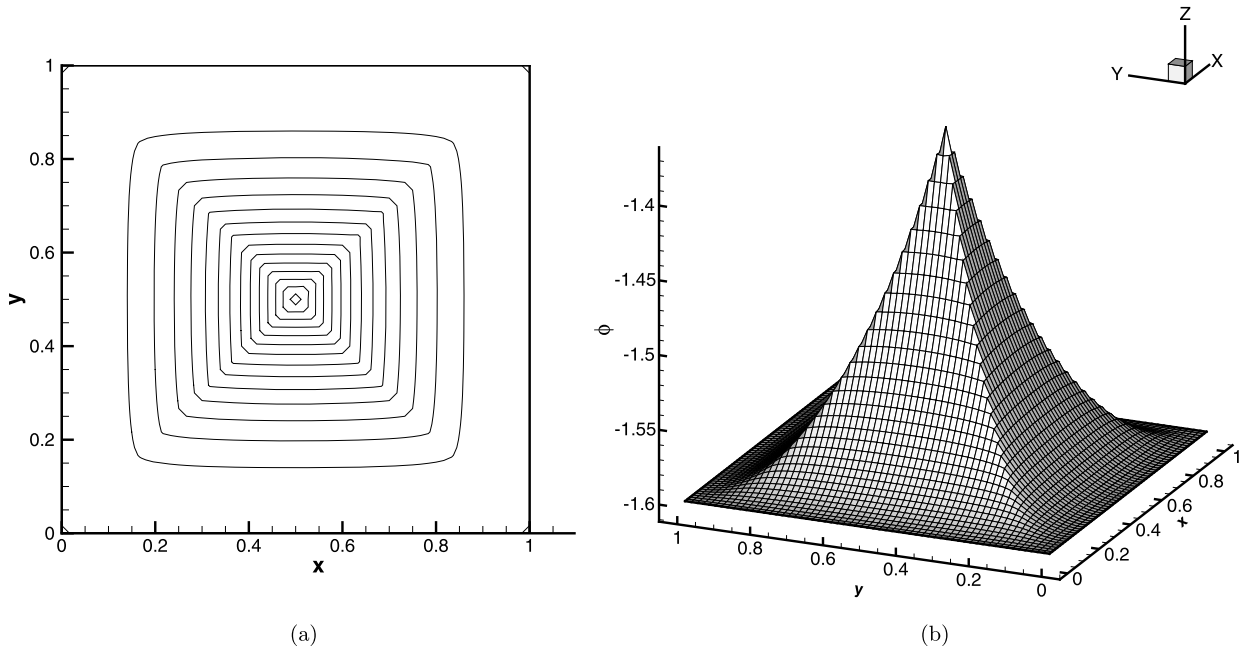

(a) (b)

Fig. 14. Eikonal equation. $t = 1$ by the HWENO schemes with 60×60 cells. Contours of the solution (a) and surface of the solution (b).

4. Conclusion

In this paper, we present a class of new HWENO schemes based on finite volume framework to directly solve the HJ equations in one and two dimensions. The main advantage of this schemes are their compactness and directly. For HWENO reconstruction, both the cell average and the first moment of the solution are evolved, and for two dimensional case, HWENO reconstruction is based on a dimension-by-dimension strategy which is the first used in HWENO reconstruction. Extensive numerical experiments in one dimensional and two dimensional cases show that the schemes developed in this paper have high order accuracy when the solution is smooth and high resolution in the region where the solution is with discontinuous derivatives. For future work, we will consider evolving the point values ϕ and its derivatives $u = \phi_x$ and $v = \phi_y$ by interpolation and their relevant PDEs, for ϕ, use monotone Hamiltonian and for u, v, use the nonconservative form of the PDEs they satisfy, to get one simpler HWENO scheme for HJ equation.

Acknowledgements

The authors thank their research group members for their valuable suggestions and comments. We also wish to thank the unnamed reviewers for their careful review works and helpful suggestions which led to an improved paper.

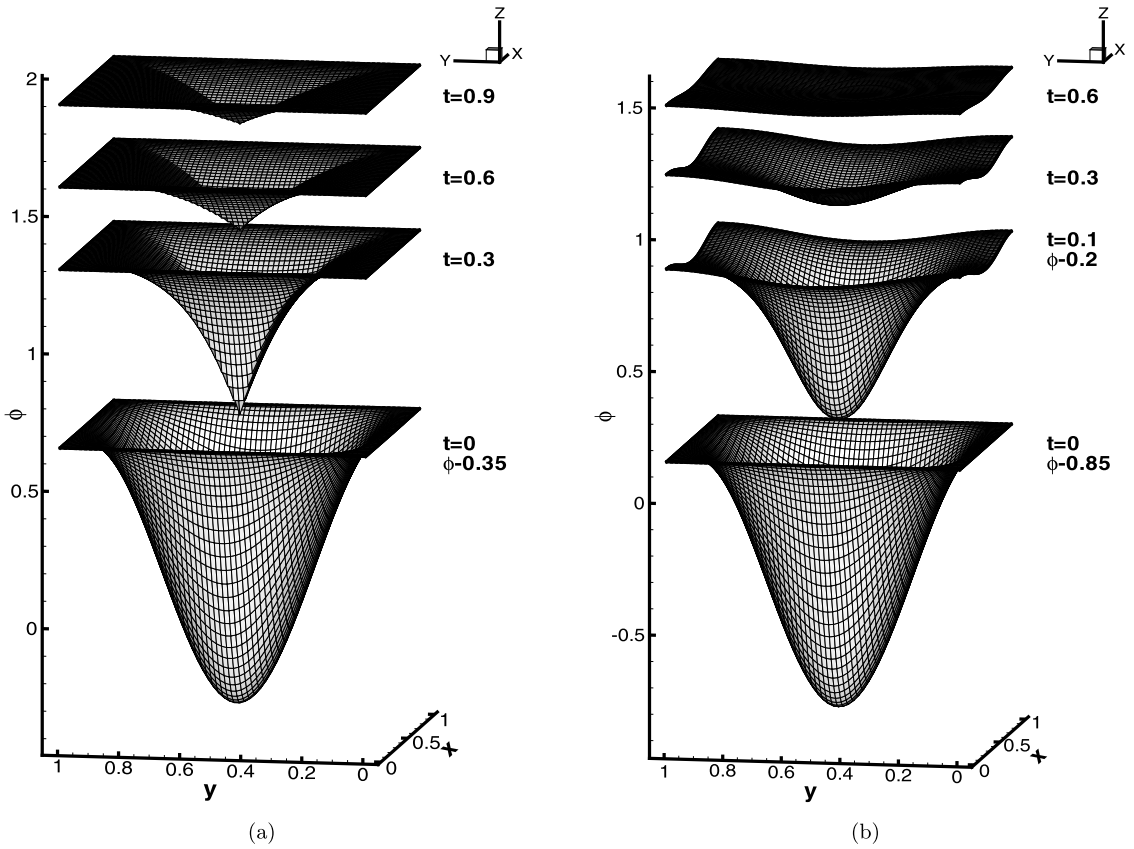

Fig. 15. Propagating surface. 60×60 cells. (a) $\varepsilon = 0$; (b) $\varepsilon = 0.1$.

References

[1] R. Abgrall, Numerical discretization of the first-order Hamilton–Jacobi equation on triangular meshes, Commun. Pure Appl. Math. 49 (1996) 1339–1373.
[2] Y. Cheng, C.W. Shu, A Discontinuous Galerkin finite element method for directly solving the Hamilton–Jacobi equations, J. Comput. Phys. 223 (2007) 398–415.
[3] Y. Cheng, Z. Wang, A new Discontinuous Galerkin finite element method for directly solving the Hamilton–Jacobi equations, J. Comput. Phys. 268 (2014) 134–153.
[4] M. Crandall, P.L. Lions, Viscosity solutions of Hamilton–Jacobi equations, Trans. Am. Math. Soc. 277 (1983) 1–42.
[5] M. Crandall, P.L. Lions, Two approximations of solutions of Hamilton–Jacobi equations, Trans. Am. Math. Soc. 43 (1984) 1–19.
[6] C. Hu, C.W. Shu, A Discontinuous Galerkin finite element method for Hamilton–Jacobi equations, SIAM J. Sci. Comput. 21 (1999) 666–690.
[7] G. Jiang, D. Peng, Weighted ENO schemes for Hamilton–Jacobi equations, SIAM J. Sci. Comput. 21 (1999) 2126–2143.
[8] G.S. Jiang, C.W. Shu, Efficient implementation of weighted ENO schemes, J. Comput. Phys. 126 (1996) 202–228.
[9] F. Lafon, S. Osher, High order two dimensional nonoscillatory methods for solving Hamilton–Jacobi scalar equations, J. Comput. Phys. 123 (1996) 235–253.
[10] F. Li, C.W. Shu, Reinterpretation and simplified implementation of a Discontinuous Galerkin method for Hamilton–Jacobi equations, Appl. Math. Lett. 18 (2005) 1204–1209.
[11] S. Osher, J. Sethian, Fronts propagating with curvature dependent speed: algorithms based on Hamilton–Jacobi formulations, J. Comput. Phys. 79 (1988) 12–49.
[12] S. Osher, C.W. Shu, High-order essentially nonoscillatory schemes for Hamilton–Jacobi equations, SIAM J. Numer. Anal. 28 (1991) 907–922.
[13] J. Qiu, Hermite WENO schemes with Lax–Wendroff type time discretizations for Hamilton–Jacobi equations, J. Comput. Math. 25 (2007) 131–144.
[14] J. Qiu, C.W. Shu, Hermite WENO schemes and their application as limiters for Runge–Kutta Discontinuous Galerkin method: one-dimensional case, J. Comput. Phys. 193 (2004) 115–135.
[15] J. Qiu, C.W. Shu, Hermite WENO schemes for Hamilton–Jacobi equations, J. Comput. Phys. 204 (2005) 82–99.
[16] J.M. Qiu, C.W. Shu, Convergence of high order finite volume weighted essentially non-oscillatory scheme and Discontinuous Galerkin method for nonconvex conservation laws, SIAM J. Sci. Comput. 31 (2008) 584–607.
[17] J. Shi, C. Hu, C.W. Shu, A technique of treating negative weights in WENO schemes, J. Comput. Phys. 175 (2002) 108–127.
[18] C.W. Shu, High order numerical methods for time dependent Hamilton–Jacobi equations, Technical Report 11, Mathematics and Computation in Imaging Science and Information Processing, Institute for Mathematical Sciences, National University of Singapore, 2007.
[19] C.W. Shu, High order weighted essentially nonoscillatory schemes for convection dominated problems, SIAM Rev. 51 (2009) 82–126.
[20] C.W. Shu, S. Osher, Efficient implementation of essentially non-oscillatory shock capturing schemes, J. Comput. Phys. 77 (1988) 439–471.
[21] Z. Xu, C.W. Shu, Anti-diffusive finite difference WENO methods for shallow water with transport of pollutant, J. Comput. Math. 24 (2006) 239–251.
[22] J. Yan, S. Osher, A local Discontinuous Galerkin method for directly solving Hamilton–Jacobi equations, J. Comput. Phys. 230 (2011) 232–244.
[23] Y.T. Zhang, C.W. Shu, High order WENO schemes for Hamilton–Jacobi equations on triangular meshes, SIAM J. Sci. Comput. 24 (2003) 1005–1030.